









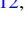

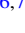






Evolution of a Peculiar Type Ibn Supernova SN 2019wep

Anjasha Gangopadhyay^{1,2} , Kuntal Misra² , Griffin Hosseinzadeh³ , Iair Arcavi^{4,5} , Craig Pellegrino^{6,7} , Xiaofeng Wang^{8,9} , D. Andrew Howell^{6,7} , Jamison Burke^{6,7} , Jujia Zhang^{10,11} , Koji Kawabata¹ , Mridweeka Singh^{12,13} , Raya Dastidar¹⁴ , Daichi Hiramatsu^{6,7,15} , Curtis McCully^{6,7} , Jun Mo⁸, Zhihao Chen⁸, and Danfeng Xiang⁸ 

¹ Hiroshima Astrophysical Science Centre, Hiroshima University, 1-3-1 Kagamiyama, Higashi-Hiroshima, Hiroshima 739-8526, Japan

² Aryabhata Research Institute of Observational Sciences, Manora Peak, Nainital 263 002 India

³ Steward Observatory, University of Arizona, 933 North Cherry Avenue, Tucson, AZ 85721, USA

⁴ The School of Physics and Astronomy, Tel Aviv University, Tel Aviv 69978, Israel

⁵ CIFAR Azrieli Global Scholars program, CIFAR, Toronto, Canada

⁶ Las Cumbres Observatory, 6740 Cortona Drive, Suite 102, Goleta, CA, 93117-5575 USA

⁷ Department of Physics, University of California, Santa Barbara, CA 93106-9530, USA

⁸ Physics Department and Tsinghua Center for Astrophysics, Tsinghua University, People's Republic of China

⁹ Beijing Planetarium, Beijing Academy of Sciences, Beijing, 100044, People's Republic of China

¹⁰ Yunnan Astronomical Observatory of China, Chinese Academy of Sciences, Kunming, 650216, People's Republic of China

¹¹ Key Laboratory for the Structure and Evolution of Celestial Objects, CAS, Kunming 650216, People's Republic of China

¹² Indian Institute of Astrophysics, 2nd Block, 100 Feet Road, Koramangala, Bengaluru, Karnataka, 560034 India

¹³ Korea Astronomy and Space Science Institute, 776 Daedeokdae-ro, Yuseong-gu, Daejeon 34055, Republic of Korea

¹⁴ Millennium Institute of Astrophysics, Nuncio Monsenor Sotero Sanz 100, Providencia, Santiago, 8320000 Chile

¹⁵ Center for Astrophysics Harvard & Smithsonian, Cambridge, Massachusetts, USA

Received 2021 October 16; revised 2022 March 23; accepted 2022 March 23; published 2022 May 11

Abstract

We present a high-cadence short term photometric and spectroscopic monitoring campaign of a type Ibn SN 2019wep, which is one of the rare SN Ibn after SNe 2010al and 2019uo to display signatures of flash ionization (He II, C III, N III). We compare the decline rates and rise time of SN 2019wep with other SNe Ibn and fast transients. The post-peak decline in all bands (0.1 mag day^{-1}) are consistent with SNe Ibn but less than the fast transients. On the other hand, the Δm_{15} values are slightly lower than the average values for SNe Ibn but consistent with the fast transients. The rise time is typically shorter than SNe Ibn but longer than fast transients. SN 2019wep lies at the fainter end of SNe Ibn but possesses an average luminosity among the fast transients sample. The peculiar color evolution places it between SNe Ib and the most extreme SNe Ibn. The bolometric light-curve modeling shows resemblance with SN 2019uo with ejecta masses consistent with SNe Ib. SN 2019wep belongs to the P cygni subclass of SNe Ibn and shows faster evolution in line velocities as compared to the *emission* subclass. The post-maximum spectra show close resemblance with ASASSN-15ed hinting it to be of SN Ib nature. The low He I CSM velocities and residual H α further justifies it and provide evidence of an intermittent progenitor between Wolf-Rayet and LBV stars.

Unified Astronomy Thesaurus concepts: [Supernovae \(1668\)](#); [Supernova dynamics \(1664\)](#); [Core-collapse supernovae \(304\)](#); [CCD photometry \(208\)](#); [Spectroscopy \(1558\)](#)

Supporting material: data behind figure

1. Introduction

Type Ibn supernovae (hereafter SNe Ibn) are a rare class of core-collapse SNe (CCSNe) undergoing interaction with hydrogen poor circumstellar medium (CSM). Interaction, in general, produces narrow emission lines—broader than H II regions but narrower than the lines arising from the outer ejecta of the SN (Pastorello et al. 2007). However, in some cases interaction happens below the photosphere without any observable narrow emission lines (e.g., Morozova et al. 2017; Andrews & Smith 2018). SNe Ibn are characterized by narrow lines of He ($\sim 2000 \text{ km s}^{-1}$) in their spectra and was introduced with the discovery of SN 2006jc (Pastorello et al. 2007). This is defined in analogy with SNe IIn, which show narrow H features (Schlegel 1990). SNe that are embedded in

dense CSM may also show short-lived narrow high ionization emission lines (at ≤ 10 days) owing to the recombination of the CSM following the shock breakout flash or through interaction of the SN ejecta with nearby CSM. These features are known as *flash features* (e.g., Gal-Yam et al. 2014; Gal-Yam 2019).

Unlike the light curves of SNe IIn, which show great photometric diversity (Nyholm et al. 2020), SNe Ibn light curves (though small in number as only less than 40 SNe Ibn are known until date; Hosseinzadeh et al. 2019) are surprisingly homogeneous with a uniform light-curve shape and decay rates of $0.05\text{--}0.15 \text{ mag day}^{-1}$ (Hosseinzadeh et al. 2017). They typically rise within a timescale of ≤ 15 days and reach a peak absolute magnitude of $M_R = -19 \text{ mag}$ (Hosseinzadeh et al. 2017), with exceptions like ASASSN-14ms, which has a peak luminosity of $M_V \sim -20.5 \text{ mag}$, lying between normal SNe Ibn and superluminous SNe (Wang et al. 2021). Pastorello et al. (2016), however, highlighted the existence of many outliers in the SN Ibn group, which are slow decliners, for example, OGLE-2012-SN-006 (Pastorello et al. 2015e) and SN 2010al (Pastorello et al. 2015a). The fast-rising and decaying nature of



Original content from this work may be used under the terms of the [Creative Commons Attribution 4.0 licence](#). Any further distribution of this work must maintain attribution to the author(s) and the title of the work, journal citation and DOI.

SNe Ibn enables their comparison with the fast transients (Drout et al. 2014; Arcavi et al. 2016; Pellegrino et al. 2022), which may hint toward their similar origin. The light curves of stripped envelope (SESNe; typically Ibs) are in general powered by radioactivity but in the case of SNe Ibn the light curves are too steep to reconcile for the amount of ^{56}Ni contributing to the radioactive luminosity (Moriya & Maeda 2016). Instead, a combination of Ni-decay and CSM interaction are required to reproduce the light curve (Karamahmetoglu et al. 2021; Wang & Li 2020; Gangopadhyay et al. 2020a).

In the past few years, one of the most perplexing questions has been regarding the progenitors giving rise to SNe Ibn explosions. The homogeneity of the light curves does not necessarily imply the homogeneity of the progenitors, which are largely dependent on the CSM configuration. Unlike SNe II where some have been linked to H-rich luminous blue variable (LBV) stars (e.g., Gal-Yam & Leonard 2009; Smith et al. 2010), there have been no direct detection of SNe Ibn progenitors to date. There are two precursor detections of massive SN Ibn progenitors—the luminous outburst of the prototypical SN Ibn 2006jc, observed 2 yr before the explosion (Foley et al. 2007; Pastorello et al. 2007; Smith et al. 2008) and the other for SN 2019uo where precursor starts ~ 340 days before the explosion and is observed over 35 days (Strotjohann et al. 2021). The progenitor of SN 2006jc is believed to be a massive star with remaining LBV properties (Pastorello et al. 2007). The stripping of the outer envelope can occur also from the massive binaries (Foley et al. 2007). Strotjohann et al. (2021) suggests that the progenitors could be Wolf-Rayet (W-R) stars that have shed their hydrogen envelopes or massive stars that are stripped by a binary partner. Recent evidence of a low-mass progenitor host has been proposed for PS1-12sk, which occurred in a non-star-forming galaxy (Sanders et al. 2013; Hosseinzadeh et al. 2019). Based on the late-time UV/optical Hubble Space Telescope images, an interacting binary progenitor scenario was inferred for SNe 2006jc and 2015G (Sun et al. 2020).

1.1. Discovery

SNe Ibn 2019wep was discovered on 2019 December 07.96979 UT by Xing Gao (Zhang et al. 2019a) in Xingming Observatory Sky Survey (C42) images at an unfiltered mag of ~ 18.2 , which was estimated by several 40 s survey images. The SN was located at R.A. = $11^{\text{h}}04^{\text{m}}36^{\text{s}}.99$, decl. = $+45^{\circ}58'39''.5$ (equinox J2000.0) (Mao et al. 2019), which is about $2''.6$ east and $27''.6$ south of the center of the host galaxy PGC 33464. Zhang et al. (2019b) obtained the classification spectrum of SN 2019wep with the 2.4 m Lijiang telescope (LJT+YFOOSC) of the Yunnan Observatories, China. The spectrum depicted a blue continuum and highly ionized *flash features* of He II, H I and C IV. This spectrum matches with that of a young SN II with signatures of interaction. Another spectrum taken a few days later shows evidence of narrow P cygni He I features classifying it as an SN Ibn. SN 2019wep is one of the rare SNe Ibn to show signatures of flash ionization after SNe 2019uo and 2010al.

1.2. Estimation of Explosion Epoch:

Mao et al. (2019) reported the non-detection of a source in archival images of Xingming Observatory Sky Survey (C42)

on 2019 May 30 (limiting mag 19.0) while the Zwicky Transient Facility (ZTF¹⁶) reported a last non-detection of the source on 2019 November 25 (MJD 58812) in *r* band at a limiting magnitude of 19.89 mag. Four pre-maximum unfiltered data points of SN 2019wep are available in TNS¹⁷, which match well with our *V*-band data. We combine the unfiltered magnitudes with our *V*-band data (since the passbands are close) and perform a parabolic fit on the combined light curve of SN 2019wep. The magnitudes are converted to flux and the fit is performed using the data up to ~ 6 days after the discovery. The best-fit coefficients are used to find the roots of the equation, i.e., the value of time for which the flux equals zero. This gives the explosion epoch to be $\text{MJD } 58824.5 \pm 2$. The error is estimated from the fitting error associated with the data.

1.3. Distance and Extinction:

Adopting $H_0 = 73 \text{ km s}^{-1} \text{ Mpc}^{-1}$, $\Omega_{\text{matter}} = 0.27$, and $\Omega_{\text{vacuum}} = 0.73$, we obtain a luminosity distance of 108.3 Mpc (corresponding to a redshift $z = 0.025$ ¹⁸) for SN 2019wep. The Milky Way extinction along the line of sight of SN 2019wep is $A_V = 0.031$ mag (Schlafly & Finkbeiner 2011). For estimating the extinction due to the host galaxy, we estimate equivalent widths (EWs) of the Na I D line in the three spectra of SN 2019wep taken on 2019 December 16, 2019 December 19, and 2019 December 24. Using the formulation by Munari & Zwitter (1997) and Poznanski et al. (2012), we estimate host galaxy $A_V = 0.0328$ mag. The estimated extinction results in matching the $(B - V)$ colors of SN 2019wep in close agreement with that of SNe 2010al and 2019uo. Thus, we adopt a total $A_V = 0.0638$ mag. We use these values of distance and extinction throughout the paper.

In this paper we aim to investigate the photometric and spectroscopic evolution of the peculiar SN Ibn 2019wep, which not only showed signatures of flash ionization but also shows some similarities with SN Ib at late phases. In Section 2, we discuss the procedure of photometric and spectroscopic data reduction. In Section 3, the photometric evolution of SN 2019wep is studied and compared with other SNe Ibn and fast transients. In Section 4, we discuss the interpretation of the observed spectral features including the late-time distinct P cygni features and unique $\text{H}\alpha$ behavior. Our conclusions are given in Section 5.

2. Data Acquisition and Reduction

We observed SN 2019wep with the 2 m Las Cumbres Observatory (LCO) telescopes in the *UBVgri* filters from ~ 3 –98 days after explosion under the Global Supernovae Project program. The photometric observations in *UBVRIugri* were also taken with the 0.8 m Tsinghua-NAOC Telescope (TNT; Huang et al. 2012), Xinglong Observatory, China. Image subtraction was done using High Order Transform of PSF AND Template Subtraction.¹⁹ The instrumental

¹⁶ <https://www.wis-tns.org/object/2019wep>; Bellm (2014); Bellm et al. (2019).

¹⁷ <https://www.wis-tns.org/object/2019wep>

¹⁸ [https://ned.ipac.caltech.edu/byname?](https://ned.ipac.caltech.edu/byname?objname=PGC33464&hconst=73&omegam=0.27&omegav=0.73&corr_z=4)

¹⁹ <https://github.com/acbecker/hotpants>

Table 1
Photometry of SN 2019wep

Date (yyyy-mm-dd)	JD (2400000+)	Phase (day)	<i>U</i> (mag)	<i>B</i> (mag)	<i>g</i> (mag)	<i>V</i> (mag)	<i>r</i> (mag)	<i>i</i> (mag)	Telescope
2019-12-12	58829.35	0.85	...	17.19 ± 0.03	17.11 ± 0.03	17.29 ± 0.03	17.42 ± 0.10	...	LCO
2019-12-12	58829.35	0.85	...	17.20 ± 0.03	17.18 ± 0.04	17.38 ± 0.04	LCO
2019-12-13	58830.41	1.91	16.49 ± 0.03	17.38 ± 0.02	17.35 ± 0.03	17.41 ± 0.03	17.48 ± 0.03	17.91 ± 0.07	LCO
2019-12-13	58830.41	1.91	16.45 ± 0.04	17.35 ± 0.03	17.28 ± 0.02	17.43 ± 0.03	17.57 ± 0.03	17.75 ± 0.07	LCO
2019-12-15	58832.36	3.86	16.86 ± 0.04	17.48 ± 0.03	17.36 ± 0.03	17.59 ± 0.04	17.62 ± 0.03	17.68 ± 0.05	LCO
2019-12-15	58832.37	3.86	16.85 ± 0.05	17.56 ± 0.03	17.28 ± 0.03	...	17.59 ± 0.03	17.63 ± 0.05	LCO
2019-12-18	58835.35	6.85	17.33 ± 0.05	18.05 ± 0.03	17.84 ± 0.02	17.93 ± 0.03	17.88 ± 0.03	18.02 ± 0.03	LCO
2019-12-18	58835.35	6.85	...	18.06 ± 0.03	17.83 ± 0.02	17.93 ± 0.04	17.86 ± 0.03	18.05 ± 0.03	LCO
2019-12-18	58835.73	7.25	...	18.34 ± 0.03	18.18 ± 0.03	17.93 ± 0.05	18.06 ± 0.02	18.05 ± 0.03	TNT
2019-12-19	58836.36	7.86	17.63 ± 0.03	18.10 ± 0.02	17.94 ± 0.01	17.97 ± 0.03	17.89 ± 0.02	17.97 ± 0.03	LCO
2019-12-19	58836.37	7.87	17.49 ± 0.03	18.13 ± 0.02	17.95 ± 0.01	17.98 ± 0.03	17.88 ± 0.02	18.07 ± 0.03	LCO
2019-12-21	58838.33	9.83	17.74 ± 0.04	18.43 ± 0.03	18.13 ± 0.01	18.16 ± 0.03	18.03 ± 0.02	18.12 ± 0.03	LCO
2019-12-21	58838.34	9.84	17.80 ± 0.04	18.35 ± 0.02	18.14 ± 0.01	18.11 ± 0.03	18.06 ± 0.02	18.18 ± 0.04	LCO
2019-12-22	58839.47	10.97	18.01 ± 0.03	18.64 ± 0.02	18.33 ± 0.01	18.27 ± 0.02	18.14 ± 0.02	18.23 ± 0.03	LCO
2019-12-22	58839.48	10.98	18.02 ± 0.03	18.62 ± 0.02	18.36 ± 0.01	18.31 ± 0.02	...	18.23 ± 0.02	LCO
2019-12-24	58841.44	13.04	18.45 ± 0.10	18.75 ± 0.03	18.55 ± 0.04	18.44 ± 0.06	18.27 ± 0.04	18.21 ± 0.07	LCO
2019-12-24	58841.44	13.04	18.37 ± 0.08	...	18.60 ± 0.03	18.34 ± 0.05	18.19 ± 0.04	18.33 ± 0.08	LCO
2019-12-27	58844.37	15.87	18.98 ± 0.06	19.27 ± 0.04	18.98 ± 0.02	18.67 ± 0.03	18.56 ± 0.03	18.55 ± 0.04	LCO
2019-12-27	58844.37	15.87	19.01 ± 0.06	19.29 ± 0.04	18.99 ± 0.02	18.70 ± 0.03	18.49 ± 0.02	18.59 ± 0.04	LCO
2019-12-27	58844.78	16.28	...	19.30 ± 0.09	19.00 ± 0.05	18.71 ± 0.04	18.50 ± 0.03	18.51 ± 0.03	TNT
2019-12-28	58845.80	17.30	...	19.37 ± 0.03	19.11 ± 0.02	18.77 ± 0.03	18.61 ± 0.02	18.52 ± 0.09	TNT
2019-12-29	58846.81	18.31	...	19.47 ± 0.05	19.28 ± 0.03	18.86 ± 0.06	18.81 ± 0.06	18.91 ± 0.09	TNT
2019-12-30	58847.78	19.28	...	19.57 ± 0.05	19.47 ± 0.07	19.05 ± 0.09	18.95 ± 0.09	...	TNT
2020-01-01	58849.82	21.32	...	20.07 ± 0.09	19.87 ± 0.07	19.07 ± 0.05	19.10 ± 0.09	18.86 ± 0.05	TNT
2020-01-02	58850.47	21.97	20.32 ± 0.24	20.42 ± 0.08	20.10 ± 0.05	19.65 ± 0.08	19.31 ± 0.07	19.49 ± 0.13	LCO
2020-01-02	58850.47	21.97	20.12 ± 0.23	20.43 ± 0.10	20.09 ± 0.05	19.64 ± 0.07	19.29 ± 0.06	...	LCO
2020-01-02	58850.75	22.25	...	20.57 ± 0.99	18.89 ± 0.05	19.48 ± 0.05	19.18 ± 0.04	19.29 ± 0.04	TNT
2020-01-03	58851.78	23.28	...	20.39 ± 0.08	20.09 ± 0.05	19.59 ± 0.05	19.29 ± 0.03	18.97 ± 0.04	TNT
2020-01-04	58852.76	24.26	...	20.57 ± 0.99	20.09 ± 0.05	19.59 ± 0.05	19.40 ± 0.04	19.11 ± 0.07	TNT
2020-01-05	58853.30	24.80	20.04 ± 0.27	20.68 ± 0.22	20.52 ± 0.14	19.86 ± 0.12	19.60 ± 0.09	19.38 ± 0.09	LCO
2020-01-05	58853.30	24.80	20.40 ± 0.32	19.89 ± 0.13	19.51 ± 0.09	19.35 ± 0.08	LCO
2020-01-06	58854.28	25.78	...	20.62 ± 0.22	20.65 ± 0.19	20.06 ± 0.14	19.48 ± 0.10	19.48 ± 0.24	LCO
2020-01-06	58854.28	25.78	...	20.41 ± 0.22	...	19.95 ± 0.13	19.41 ± 0.08	20.53 ± 0.15	LCO
2020-01-14	58862.44	33.94	...	20.73 ± 0.24	...	20.63 ± 0.20	19.47 ± 0.16	...	LCO
2020-01-14	58862.46	33.94	20.32 ± 0.17	19.96 ± 0.21	...	LCO
2020-01-18	58866.44	37.94	...	21.49 ± 0.24	21.51 ± 0.17	20.63 ± 0.16	20.01 ± 0.09	19.88 ± 0.11	LCO
2020-01-18	58866.44	37.94	...	21.28 ± 0.21	21.10 ± 0.12	20.53 ± 0.13	20.08 ± 0.09	19.88 ± 0.11	LCO
2020-01-24	58872.48	43.98	...	21.34 ± 0.18	21.27 ± 0.10	21.28 ± 0.14	20.15 ± 0.08	19.91 ± 0.11	LCO
2020-01-24	58872.49	43.99	...	21.48 ± 0.25	21.28 ± 0.11	20.89 ± 0.12	20.18 ± 0.07	19.94 ± 0.11	LCO
2020-01-28	58876.43	47.93	...	21.66 ± 0.33	21.47 ± 0.16	20.79 ± 0.16	20.34 ± 0.12	20.31 ± 0.16	LCO
2020-01-28	58876.44	47.94	...	21.84 ± 0.28	21.66 ± 0.24	20.77 ± 0.28	20.29 ± 0.08	...	LCO
2020-01-28	58876.48	47.98	...	21.80 ± 0.33	...	20.76 ± 0.13	LCO
2020-01-28	58876.48	47.98	...	21.37 ± 0.23	...	20.84 ± 0.17	LCO
2020-02-01	58880.47	51.97	...	21.39 ± 0.24	21.43 ± 0.12	20.66 ± 0.12	20.39 ± 0.10	20.20 ± 0.13	LCO
2020-02-01	58880.48	51.98	...	21.52 ± 0.24	21.56 ± 0.16	20.81 ± 0.16	20.42 ± 0.11	20.33 ± 0.15	LCO
2020-02-08	58887.41	58.91	...	21.51 ± 0.53	21.34 ± 0.28	21.21 ± 0.49	20.34 ± 0.19	20.38 ± 0.25	LCO
2020-02-08	58887.41	58.93	21.88 ± 0.42	20.67 ± 0.34	21.57 ± 0.44	21.76 ± 0.24	LCO
2020-03-15	58923.61	95.11	...	22.67 ± 0.39	22.27 ± 0.31	22.05 ± 0.45	21.99 ± 0.43	21.88 ± 0.13	TNT

Note. The phase is measured with respect to V -max ($MJD_{\max} = 58828.5$).

magnitudes were estimated using DAOPHOT.²⁰ The LCO image subtraction and photometry were done with `lco_gtsn_pipe`²¹ (see Valenti et al. 2011, 2016). The instrumental SN magnitudes in *gri* bands and UVB bands were calibrated with respect to the Sloan Digital Sky Survey catalog and Landolt standard fields, respectively.

The photometry of SN 2019wep is presented in Table 1.

The spectroscopic observations of SN 2019wep were taken at 9 epochs spanning up to ~ 22 days after explosion with the 2.0 m FTN and FTS telescopes of the LCO and 2.4 m LJT of Yunnan Observatories, China. The 1D wavelength- and flux-calibrated spectra were extracted using the `floydsspec` pipeline²² (Valenti et al. 2014) for the LCO data. Spectroscopic data of the LJT telescope was reduced using the APALL task in IRAF²³ followed by wavelength and flux calibration. The slit

²⁰ Dominion Astrophysical Observatory Photometry.

²¹ https://github.com/svalenti/lco_gtsn_pipe

²² <https://github.com/svalenti/FLOYDSSpecPipeline>

²³ Image Reduction and Analysis Facility.

Table 2
Log of Spectroscopic Observations of SN 2019wep

Phase	Telescope	Instrument	Range Å
-2.9	2.0 m LJT	YFOSC	3400–7600
-2.9	2.0 m LJT	YFOSC	3400–7600
-2.0	2.0 m FTN	FLOYDS spectrograph	3400–9500
-1.0	2.0 m FTN	FLOYDS spectrograph	3400–9500
0.0	2.0 m FTN	FLOYDS spectrograph	3400–9700
1.4	2.0 m LJT	YFOSC	3400–7600
5.0	2.0 m FTN	FLOYDS spectrograph	3400–9700
7.2	2.0 m LJT	YFOSC	3400–7600
8.0	2.0 m FTN	FLOYDS spectrograph	3400–9500
12.3	2.0 m LJT	YFOSC	3400–7600
13.0	2.0 m FTN	FLOYDS spectrograph	3400–9500
18.3	2.0 m LJT	YFOSC	3400–7600

Note. The phase is measured with respect to V -max ($\text{MJD}_{\text{max}} = 58828.5$).

loss corrections were done by scaling the spectra to the photometry. Finally, the spectra were corrected for the heliocentric redshift of the host galaxy. The log of spectroscopic observations is given in Table 2.

3. Photometric Evolution of SN 2019WEP

The multiband light-curve evolution of SN 2019wep is shown in Figure 1. Even though our observations were unable to trace the light-curve maximum, four pre-maximum unfiltered data points were reported in TNS, which we combine with our V -band data to perform a polynomial fit on the early data up to 8 days. A derivative of the flux values tending to zero is used to estimate the light-curve maximum which occurs at $\text{MJD } 58828.5 \pm 2$ days. The error in the obtained values is the fitting error associated with the light curve. The maximum magnitude in the V band is estimated by fitting a cubic spline function in the light-curve data up to ~ 10 days. This results in a peak absolute magnitude of $M_V = -18.26 \pm 0.20$ mag where the estimated error accounts for the contribution of error in magnitude, redshift, and interpolation errors. Even though most of the SNe Ibn have covered the r -band maximum, which is also the case of our comparison sample, we use days since V -maximum as a reference epoch throughout the study because of a better sampling in the V band.

For estimating the peak absolute magnitude in r and i bands, we select the first 30 days phase bin and perform a linear fit on the light curve as suggested by Hosseinzadeh et al. (2017) where the intercept gives a measure of the peak absolute magnitude. The peak absolute magnitudes for SN 2019wep are estimated to be $M_r = -18.18 \pm 0.95$ mag and $M_i = -17.98 \pm 0.99$ mag. The error on the peak magnitude is estimated from the estimated error on the peak date, the standard errors on the slope and intercept, and the slope-intercept covariance of the fit. We want to remark that the extrapolated peak only provides a limit on the magnitudes, and thus large error bars are associated with the estimation.

The rise time of an object is generally estimated as the difference between the estimated explosion epoch and the maximum. In the case of SN 2019wep we estimate the rise time to be 4 ± 3 days. The error in rise time is the error in the explosion epoch and the epoch of maximum propagated in quadrature. The rise time of SN 2019wep indicates that it is one of the fast-rising members among the SNe Ibn subclass and has

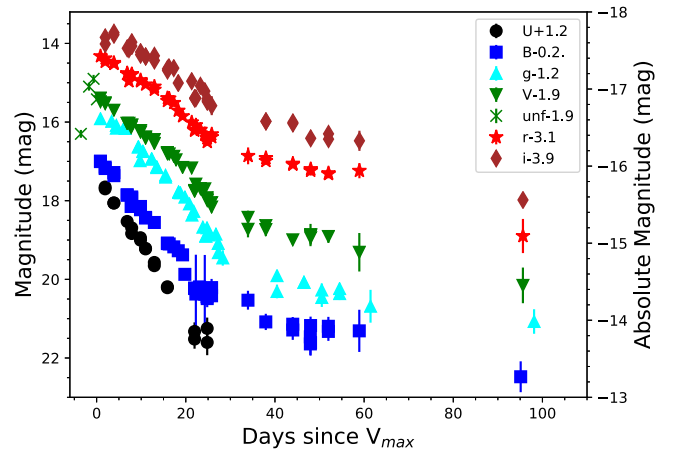


Figure 1. $UBgVri/unfiltered$ light-curve evolution of SN 2019wep.

a good match with SN 1999cq (see Table 4; Hosseinzadeh et al. 2017; Matheson et al. 2000).

The r -band light curve of SN 2019wep, between 0 and 30 days post maximum, has a decay rate of 0.088 ± 0.002 mag day $^{-1}$. The V - and i -band light curves follow approximately the same decline rate as the r band and is roughly comparable to the SNe Ibn sample, i.e., 0.1 mag day $^{-1}$, of course with few exceptions (Hosseinzadeh et al. 2017). The g - and B -band light curves decay slightly faster with a rate of $\sim 0.145 \pm 0.003$ mag day $^{-1}$. Given the peak luminosity and decline rate, SN 2019wep also seems to follow the peak luminosity-decline rate relation of SNe Ibn proposed by Wang et al. (2021) concluding that more luminous SNe tend to have slower post-peak decline rates because of different CSM configurations.

Fast transients are the group of objects that rise and fade in brightness on timescales much shorter than those of other SNe (Drout et al. 2014; Arcavi et al. 2016; Pellegrino et al. 2022; Maeda & Moriya 2022). Their progenitor systems are uncertain and they have a featureless blue continuum similar to most SNe Ibn. The fast transients were an underrepresented class with a very few known examples (Ofek et al. 2010; Kasliwal et al. 2010) that were discovered by chance and displayed diverse observational properties. The recent high-cadence surveys (Pursiainen et al. 2018; Tampo et al. 2020; Andreoni et al. 2021) have allowed for a systematic search of fast transients. Using the ZTF sample, Ho et al. (2021) distinguished fast transients into three categories—(i) subluminous SN Iib/Ic population, (ii) luminous SN Ibn population, and (iii) fast and blue optical transients. These studies have shown similarities between SNe Ibn and fast transients that are mostly powered by ejecta interacting with He-rich CSM. Moreover, SNe Ibn and fast transients show similar rise times, peak luminosity, and decay rates (Clark et al. 2020; Xiang et al. 2021). Motivated by their similarity, we compare the absolute magnitude light curves of SN 2019wep in different bands with a sample of SNe Ibn (Hosseinzadeh et al. 2017) and fast transients (Drout et al. 2014) in the top and bottom panels, respectively, of Figure 2. The comparison sample has well covered peaks in the g , r , i bands, which are missed in SN 2019wep. The only peak coverage in SN 2019wep is in the V band. We plot the V -band absolute magnitude along with the r band in the top middle panel of Figure 2 to show the comparison of peak magnitudes. The limiting peak absolute

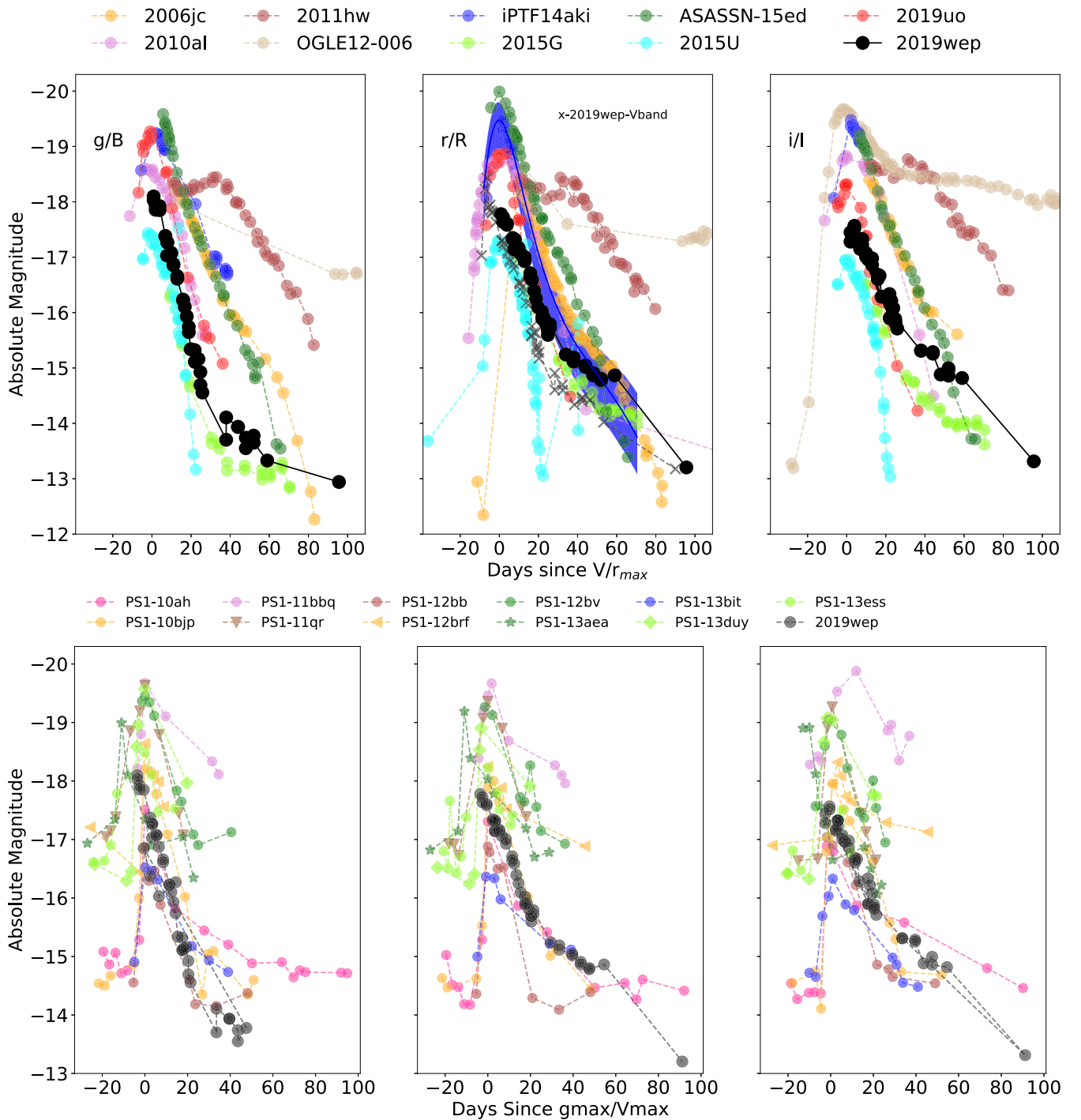


Figure 2. *gri* light-curve comparisons of SN 2019wep with a sample of SNe Ibn (Hosseinzadeh et al. 2017) in the top three panels and with a group of fast transients in the bottom three panels taken from Drout et al. 2014. The SNe Ibn comparison sample includes SNe 2006jc (Foley et al. 2007; Pastorello et al. 2007), 2010al (Pastorello et al. 2015b), OGLE-SN-006 (Pastorello et al. 2015e), 2011hw (Pastorello et al. 2015b), iPTF14aki (Hosseinzadeh et al. 2017), 2015U (Shivvers et al. 2016; Hosseinzadeh et al. 2017), 2015G (Hosseinzadeh et al. 2017), ASASSN-15ed (Pastorello et al. 2015c), and 2019uo (Gangopadhyay et al. 2020a). Phase is plotted with respect to maxima for all the panels.

magnitudes of SN 2019wep in the *r* and *i* bands are estimated by performing a linear fit as mentioned previously. We also estimate the 0–30 day decay rates of the sample of fast transients and find that it typically lies between 0.03 and 1 mag day⁻¹. This indicates that the SN 2019wep light curves evolve faster than a prototypical SN II, i.e., an SNe IIP/III with a post-plateau decay rate of 0.01 mag day⁻¹ (Lyman et al. 2016; Bose et al. 2018), but has an evolution consistent with the

categorized fast transients and lies at the faster decay end of SNe Ibn.

The top middle panel of Figure 2 also shows the normalized light curve of SNe Ibn (taken from Hosseinzadeh et al. (2017), comprising 95% of the SNe Ibn data) by the blue shaded region in the *r* band. The normalized light curve was generated by first normalizing all light curves by their estimated peak magnitudes and using a Gaussian process to estimate the average light

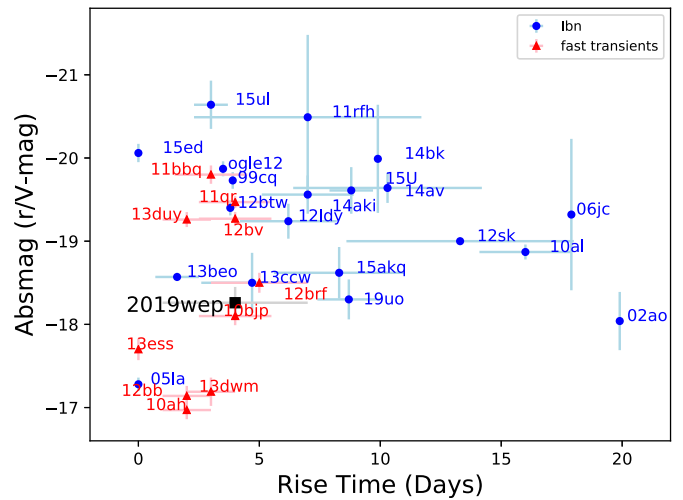
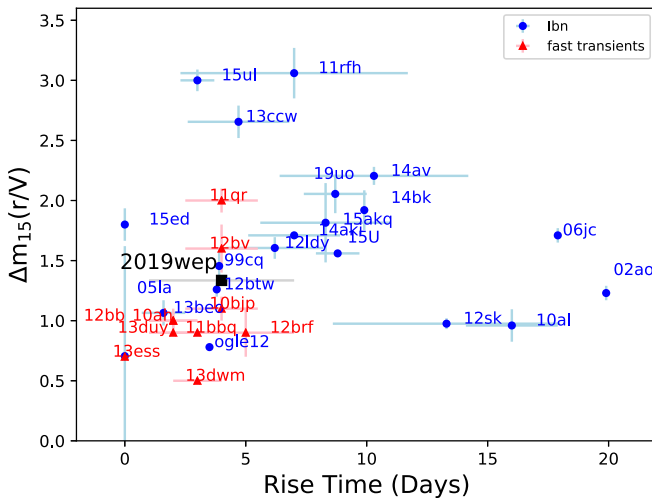


Figure 3. The Δm_{15} vs. rise time (left panel) and absolute magnitude vs. rise time (right panel) correlation plots of SN 2019wep with a sample of SNe Ibn and fast transients. The sample of type SNe Ibn has been taken from Hosseinzadeh et al. (2017) and Gangopadhyay et al. (2020a) and the sample of fast transients are taken from Drout et al. (2014).

curve. We see that the light-curve shape of SN 2019wep is well matched with that of SNe 2010al, 2019uo, and ASASSN-15ed and the brightness is comparable to iPTF14aki. The estimated peak magnitude in SN 2019wep is toward the lower brightness limit of the SNe Ibn sample. Since non-detections were not included in generating the normalized light curve by Hosseinzadeh et al. (2017), the template is biased toward a brighter and shallower evolution at early times with longer rise times of SNe Ibn. In comparison to the fast transients, SN 2019wep lies at an average brightness. The light-curve shape matches well with one of the fast transient PS1-10ah.

Figure 3 shows the correlation plots of SNe Ibn and fast transients where the Δm_{15} and absolute magnitude are plotted against the rise time. The plot indicates that the rise time of SN 2019wep is shorter (even though large error bars are associated with these estimations) with respect to the rise time estimates of other SNe Ibn. The rise time of SN 2019wep is slightly larger than the average value of the fast transients. The Δm_{15} value matches well with SN 1999cq and is lower compared to other SNe Ibn. Even though rise times indicate that SN 2019wep lies in the faster end of the SNe Ibn sample, still, we remark that the light curves do not evolve faster than the group of fast transients. SN 2019wep is fainter than most of the SNe Ibn, whereas it is of average brightness with respect to the fast transients.

We also compare the $B-R/r$ color evolution of SN 2019wep with a number of SNe Ibn, which usually show heterogeneity in their color evolution (bottom plot of Figure 4). We see that SN 2019wep shows a color evolution similar to SNe 2010al, ASASSN-15ed, and 2019uo in early times but later on transitions to blue. The $B-r$ color of SN 2019wep increases up to 1.58 mag in ~ 52 days post maximum, and subsequently becomes blue at ~ 93 days. SN 2019wep continues to become redder for a longer duration of time than other SNe Ibn. For, SNe 2010al, iPTF14aki, 2019uo, ASASSN-15ed, and 2019wep the $B-r$ color increases up to ~ 1 mag, ~ 40 days post maximum. At similar epochs, the color evolution of SN 2006jc was extremely blue (-0.5 mag). The transition to the redder colors for SNe 2019wep indicates that it shows the characteristic of not a typical Ibn SN, but the one which shows a close resemblance to an SN Ib with time. This is in good

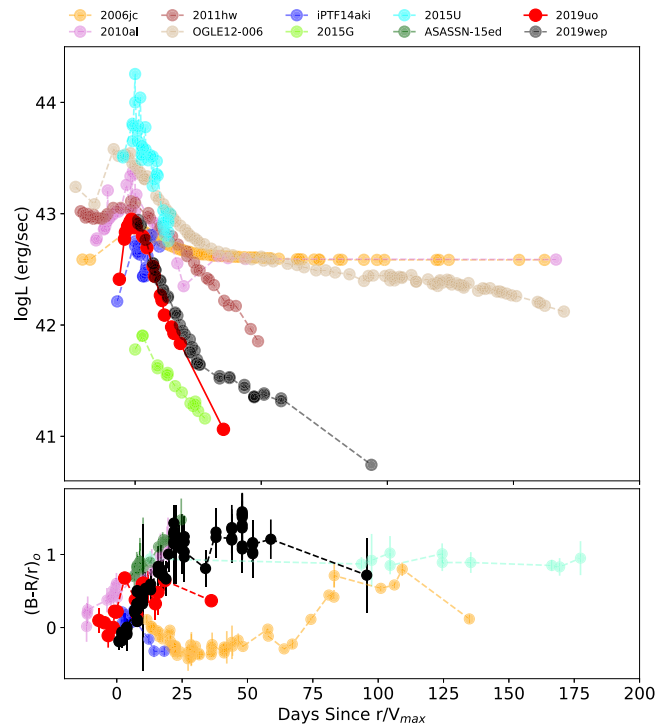


Figure 4. Complete bolometric light curve and $B-R/r$ color curve of SN 2019wep. The comparison sample includes SNe 2006jc (Pastorello et al. 2007; Foley et al. 2007), 2010al (Pastorello et al. 2015b), OGLE-SN-006 (Pastorello et al. 2015e), 2011hw (Pastorello et al. 2015b), iPTF14aki (Hosseinzadeh et al. 2017), 2015U (Shivers et al. 2016; Hosseinzadeh et al. 2017), 2015G (Hosseinzadeh et al. 2017), ASASSN-15ed (Pastorello et al. 2015c), and 2019uo (Gangopadhyay et al. 2020a).

agreement with the P cygni spectroscopic features that transition from narrow to broad, indicating a He-rich circumstellar shell around the progenitor star along with optically thick CSM. The late redder colors for SN 2006jc (Pastorello et al. 2007) and OGLE-2012-SN-006 (Pastorello et al. 2015e) are indicative of dust formation.

To construct the bolometric light curve of SN 2019wep between the UV and IR bands, we used the SuperBol code

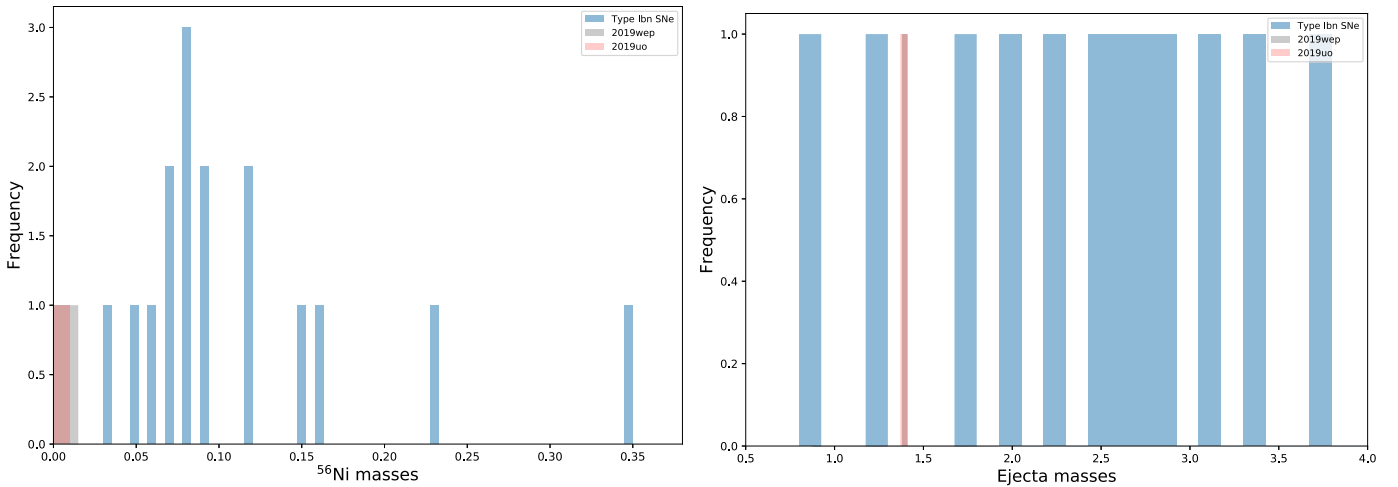


Figure 5. Histograms showing the comparison of the ^{56}Ni masses and the ejecta masses of SNe 2019wep and 2019uo with a statistical sample of SNe Ib taken from Taddia et al. (2018) and Prentice et al. (2019).

(Nicholl 2018). The missing UV and near-IR data was supplemented by extrapolating the spectral energy distributions (SEDs) using the blackbody approximation and direct integration method as described in Lusk & Baron (2017). A linear extrapolation was performed in the UV regime at late times. The estimated limiting peak bolometric luminosity of SN 2019wep is $8.8 \times 10^{42} \text{ erg s}^{-1}$ (top panel of Figure 4). The bolometric light curves of other SNe Ibn are also shown in the figure. The overall light curve of SN 2019wep matches well with that of SN 2019uo (peak luminosity $\sim 8.9 \times 10^{42} \text{ erg s}^{-1}$). Gangopadhyay et al. (2020a) inferred that SN 2019uo was best described with a $^{56}\text{Ni} + \text{CSM}$ model, which can be assumed to be consistent with SN 2019wep (given that both SNe have similar peak luminosities) with a ^{56}Ni mass of $\sim 0.01^{+0.003}_{-0.002} M_{\odot}$.

The bolometric light-curve modeling of SN 2019wep has been performed in the work by Pellegrino et al. (2022), which we briefly summarize in this section. The physical parameters were derived from a best-fit hybrid model using the MINIM code (Chatzopoulos et al. 2013), which finds self-similar solutions to the propagation of forward and reverse shocks generated by the interaction between the SN ejecta and optically thick CSM as described by Chevalier (1982). The CSM has as its free parameters an inner radius R_{ej} , mass M_{CSM} , and density ρ_{CSM} , which has an assumed power-law form with index $n = 12$ in the outer region, and $n = 0$ in the inner region. In addition to the CSM interaction, radioactive decay of ^{56}Ni is used as an additional luminosity source. Constant optical and gamma-ray opacities are also assumed.

Pellegrino et al. (2022) find that the bolometric evolution of SN 2019wep can be well explained by CSM interaction plus radioactive decay, following the mechanism by Chatzopoulos et al. (2013). The best-fit model light curve to the data is shown in their Figure 1, with model parameters listed in their Table 6 (Pellegrino et al. 2022). This model has very similar CSM and ejecta parameters to those of SN 2019uo, including values of R_{ej} , ejecta mass M_{ej} , M_{CSM} , ^{56}Ni mass M_{Ni} , and ρ_{CSM} , which are consistent with one another. The best-fit parameters of SN 2019uo from Chatzopoulos et al. (2013) differ from those presented in Gangopadhyay et al. (2020a), due to the fact that different assumptions were made between the models used in these two studies, including assumed CSM density power-law indices. Nevertheless, the inferred parameters for these two

SNe Ibn indicate that they likely share similar CSM and explosion properties, which was expected because both members belong to the P cygni class of SNe Ibn with flash-ionized features. A direct comparison of SNe Ibn with SNe Ib is not possible because of the difference in the luminosity powering mechanism. We see, however, that even though the obtained ^{56}Ni masses are lower than the canonical SESNe (Maeda & Moriya 2022), the ejecta masses obtained are consistent with many SNe Ib as deciphered from the statistical analysis of Lyman et al. (2016) and Prentice et al. (2016). This is also seen in the histograms (Figure 5), which compare SNe 2019uo and 2019wep with the statistical sample of SNe Ib taken from Prentice et al. (2019) and Taddia et al. (2018). We see that both SNe 2019uo and 2019wep lie at the lower limit of ^{56}Ni mass while the ejecta masses are quite consistent with the sample. So, we can expect the appearance of P cygni spectroscopic features and broadening of the features with time. Also, since our obtained light curves are consistent with other SNe Ibn, the ejecta properties are expected to be within the canonical sample of SESNe (Maeda & Moriya 2022). It is interesting, however, to note that the ^{56}Ni masses of SNe 2019uo and 2019wep are very low. Although, there is no systematic study being done that compares the ^{56}Ni masses with the ejecta masses for a group of SNe Ibn, in a recent study by Perley et al. (2022), very low ^{56}Ni mass ($\leq 0.03 M_{\odot}$) was estimated in SN Icn 2021csp using late-time photometric upper limits. Analysis of three recent SNe Icn 2021csp (Perley et al. 2022), 2019hgp (Gal-Yam et al. 2022), and 2021ckj (Pastorello et al. 2021) has shown that the velocities, abundance patterns, and luminosities of SNe Ibn versus SNe Icn are parallel and share a similar W-R progenitor. It is likely that the low ^{56}Ni mass yields are due to significant fallback onto the central remnant after the explosion, which only unbound a small fraction of the ^{56}Ni produced. This could be a possible scenario if a massive W-R star undergoes only a partially successful explosion. Our estimated values of ^{56}Ni mass from the best-fit model light curves are lower than those of normal SNe Ibc but are consistent with those of SNe Icn (such as SN 2021csp), indicating that there was substantial fallback after the explosion (as claimed by Perley et al. 2022). This scenario also explains a reduced ejecta mass, which could explain why the ejecta mass of SN 2019wep is comparable to SNe Ib even if the progenitor

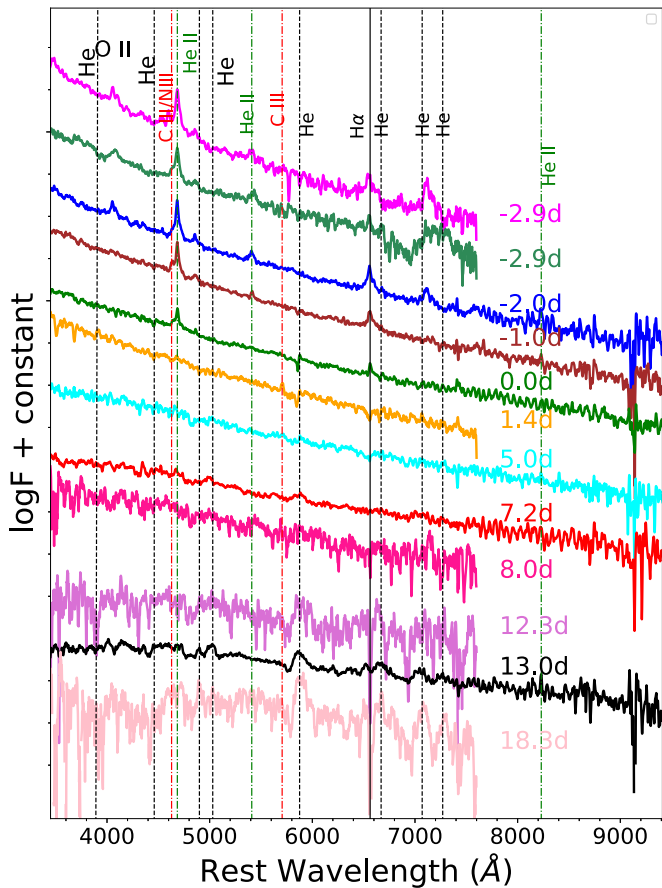


Figure 6. Spectral evolution of SN 2019wep from -2.9 to 18.3 days post maximum. Prominent He features are seen in the early spectra. Flash ionization signatures of He II, C III, and N III are also seen. Broadening of He lines become prominent with time.

(The data used to create this figure are available.)

is massive ($\geq 20 M_{\odot}$). The other scenario could be the explosion of an ultra-stripped low-mass star, but the total ejecta mass of SN 2019wep is too high to justify this case.

4. Spectral Evolution

We present the spectral evolution of SN 2019wep from -2.9 to 18.3 days post maximum (Figure 6). The first few spectra of SN 2019wep are very similar to SNe 2010al and 2019uo with a distinct blue continuum. The presence of this blue continuum also makes it similar to fast transients (Drout et al. 2014; Pellegrino et al. 2022). We fit a blackbody on the first three spectra (-2.9 , -2.0 , and -1.0 days) of SN 2019wep, which show that the photospheric temperature varies between $22,000$ and $15,000$ K. However, we want to remark that the SEDs of these SNe peak in the UV regime (Drout et al. 2014) and the temperature will essentially depend on the UV brightness of the object. As such, the temperature derived from the photometry is uncertain owing to the lack of UV observations. A narrow $H\alpha$ emission is seen in the early spectrum of SN 2019wep with a velocity of ~ 3000 km s^{-1} , which is most likely due to interstellar gas in the host galaxy and some contribution from SN, which we will explain in detail in later sections. We see typical features of emission in SN 2019wep around ~ 4660 Å in the first five spectra (-2.9 to 0.0 days). The emission components are double peaked with

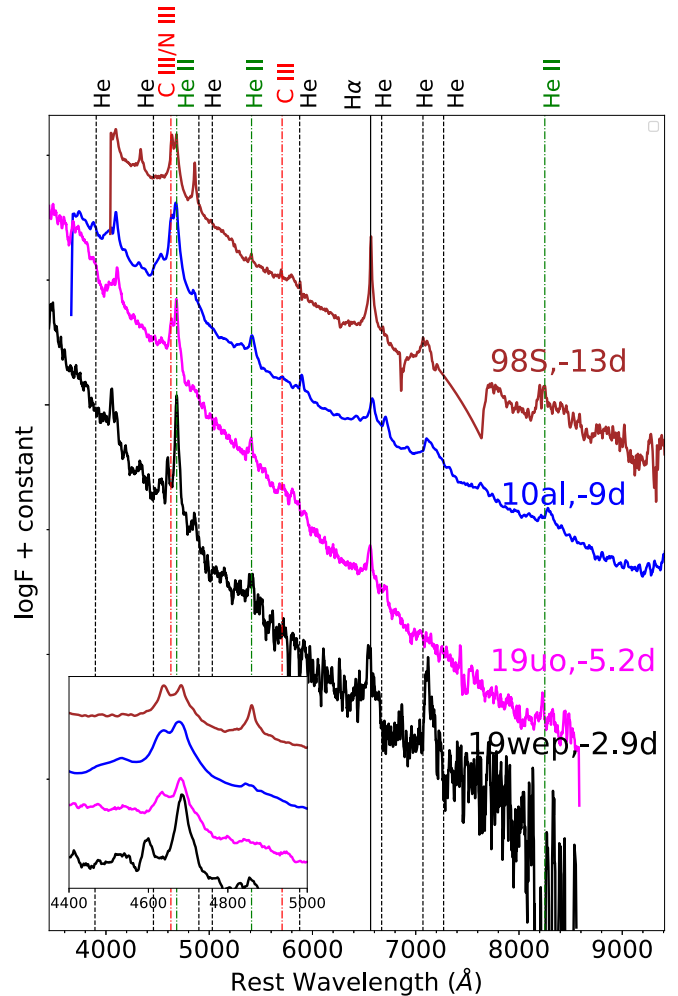


Figure 7. Spectral comparison of SN 2019wep at -2.9 days with SNe 1998S (Fassia et al. 2001), 2010al (Pastorello et al. 2015b), and 2019uo (Gangopadhyay et al. 2020a). Prominent flash ionization features are marked.

two distinct transitions, the blue component peaking at 4643 Å and the red component peaking at 4682 Å. The red component at 4682 Å is due to He II at 4686 Å, whereas the blue component arises from a blend of C III 4648 Å and N III 4640 Å. A very weak, less prominent doubly ionized C III feature at 5696 Å is also seen. These signatures are interpreted as He-rich signatures in a flash-ionized CSM (Gal-Yam 2014; Pastorello et al. 2015a). Previously flash ionization signatures of C III were seen in PTF12ldy and iPTF15ul (Hosseinzadeh et al. 2017). In SNe Ibn 2010al and 2019uo the flash ionization signatures of both C III and He II, typical of SNe II, are seen. The presence of such lines indicate that they could likely have originated from W-R winds (Cooke et al. 2010; Silverman et al. 2010). Flash-ionized signatures were previously noted in SNe IIn (e.g., SN 1998S; Fassia et al. 2001 and SN 2008fq; Taddia et al. 2013). Groh (2014) reverted the W-R progenitor scenario through the estimation of the physical parameters of SN IIb 2013cu and found that the progenitor is not a W-R star even though the flash-ionized features showed W-R-like lines. A He II 5411 Å feature with a velocity between 1413 and 1483 km s^{-1} is also seen in the very early spectra (-2.9 to 0.0 days) of SN 2019wep. In the early spectra, an absorption feature is seen close to ~ 4000 Å, which is most likely due to the presence of O II and He II features, respectively.

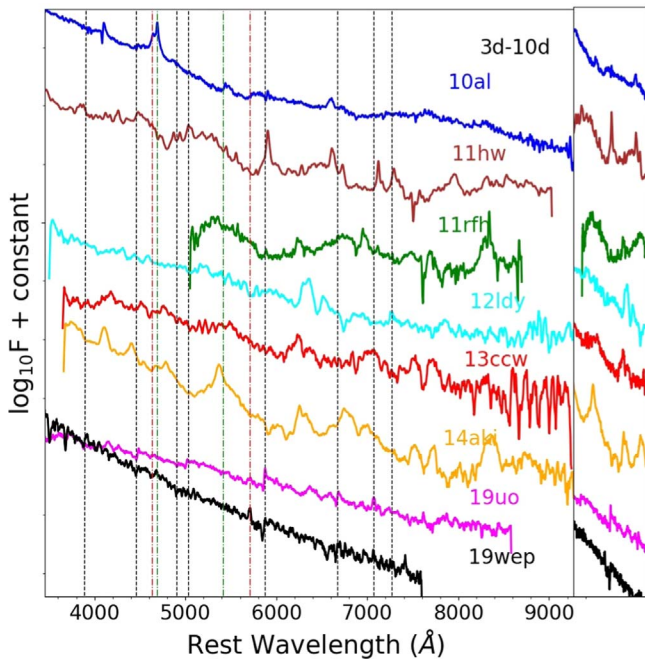


Figure 8. Comparison of the spectrum of SN 2019wep to other SNe Ibn. SN 2019wep belongs to the P cygni subclass and shows a close resemblance to SNe 2010al and 2019uo. The data for this are taken from SNe 2010al (Pastorello et al. 2015a), 2011hw (Pastorello et al. 2015a), PTF11rffh (Hosseinzadeh et al. 2017), PTF12ldy (Hosseinzadeh et al. 2017), LSQ13ccw (Pastorello et al. 2015b), iPTF14aki (Hosseinzadeh et al. 2017), and 2019uo (Gangopadhyay et al. 2020a). The right panel of the plot shows the P cygni and the emission lines of the He I 5876 Å feature.

Figure 7 shows a comparison of the early spectra of SNe 1998S (type IIn), 2010al (type Ibn), and 2019uo (type Ibn) with SN 2019wep. It is interesting to note that SN 2019wep shows the strongest flash features in the early spectrum as compared with other SNe Ibn. The spectrum of SN 2010al shows only C III features around 4650 Å, and SN 2019wep shows C III features around 4650 and at 5696 Å in agreement with SN 2019uo. The inset in Figure 7 highlights these features, which also indicates that SN 2019wep shows the most significant He II feature.

As the SN evolves further (0.0 days), we see a distinct He I P cygni feature that is superimposed on a broader base (the continuum is not flat). The flash ionization spectral signatures vanishes with time and disappears on 1.4 days. From 5.0–18.3 days, features of Ca II, Si II, and Na I D also start developing (see Figure 6). Figure 8 shows the spectral comparison of SN 2019wep with other SNe Ibn in the phase range between 3 days and 10 days post maximum. At similar phases, the He I 5876 Å feature of SN 2019wep is similar to that identified in SN 2010al and SN 2019uo with a narrow P cygni feature while other members show a prominent emission profile. Also, the continuum of SN 2019wep is bluer as compared to all other SNe of the comparison sample. However, the He I P cygni feature of SN 2019wep is broader than SNe 2010al and 2019uo, and is superimposed over a broader emission line. On the other hand, the He I P cygni profile in SN 2010al is over a flat continuum. The flash ionization signatures in SN 2019wep have vanished in this phase, but in SN 2010al these signatures are still visible. The spectral signatures of SN 2019wep (especially He I as shown in zoomed version in the right inset) indicates that SN 2019wep belongs to the P cygni subclass.

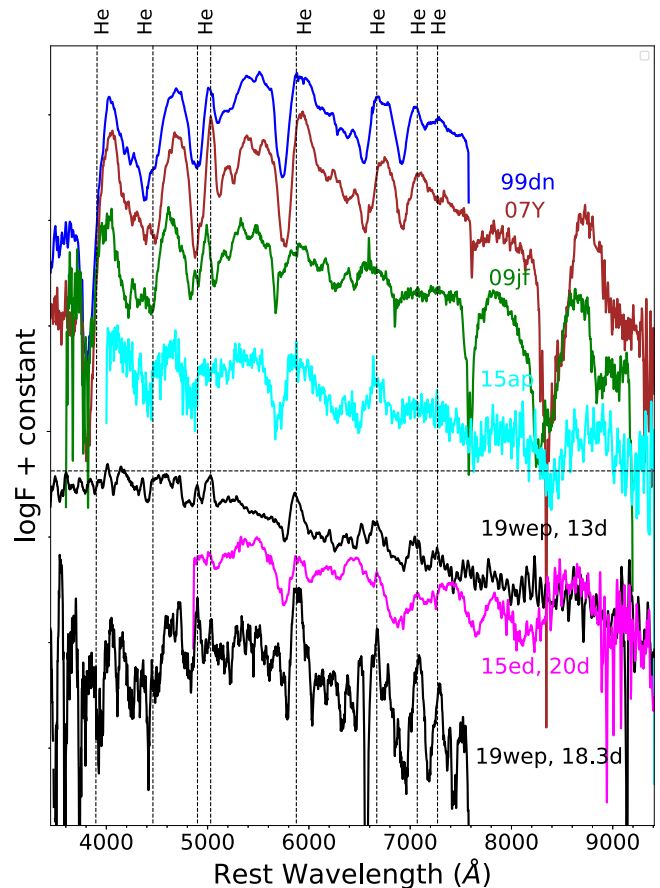


Figure 9. Comparison of the spectrum of SN 2019wep to other SN Ib and a transitioning SN Ibn ASASSN-15ed. The data are taken from ASASSN-15ed (Pastorello et al. 2015c), SNe-1999dn (Benetti et al. 2011), 2007Y (Stritzinger et al. 2009), 2009jf (Valenti et al. 2011), and 2015ap (Gangopadhyay et al. 2020b).

We see distinct broad emission lines of He I developing from 7.2–18.3 days, indicating similarity to an SN Ib. For a more evident comparison, we plot the spectrum of SN 2019wep in Figure 9 with SN Ibn ASASSN-15ed (Pastorello et al. 2015c) and a few prototypical SNe Ib between 15 and 20 days after maximum. A comparison of the He I velocity of SN 2019wep shows that it has a typical absorption FWHM velocity of $\sim 5000 \pm 1000 \text{ km s}^{-1}$. At similar epochs, the FWHM velocity of ASASSN-15ed is $6300 \pm 1000 \text{ km s}^{-1}$, which is comparable to that of SN 2019wep. This is less than the typical SN Ib velocity of our comparison sample, which has absorption trough velocity between 7000 and 9000 km s^{-1} . The major difference observed between SNe Ibn and SNe Ib spectra is that SNe Ibn have more symmetric profiles, while in SNe Ib the absorption dominates over the emission. Additionally, the absorption components of He I in SN 2019wep are almost similar to SNe Ib spectra suggesting a higher kinetic energy per mass unit in the SN ejecta, especially in the late phases of SNe Ibn that develop broad lines (Pastorello et al. 2015c). The simultaneous presence of a very narrow feature at early phases and transitioning to broad features suggests that these features arise from different emitting regions: the broader He I P cygni features are likely a signature of the SN ejecta, while the narrow He I P cygni lines are generated in the unperturbed, Herich CSM. At early phases, the narrow lines are formed in the photosphere located in a dense shell. This shell is either

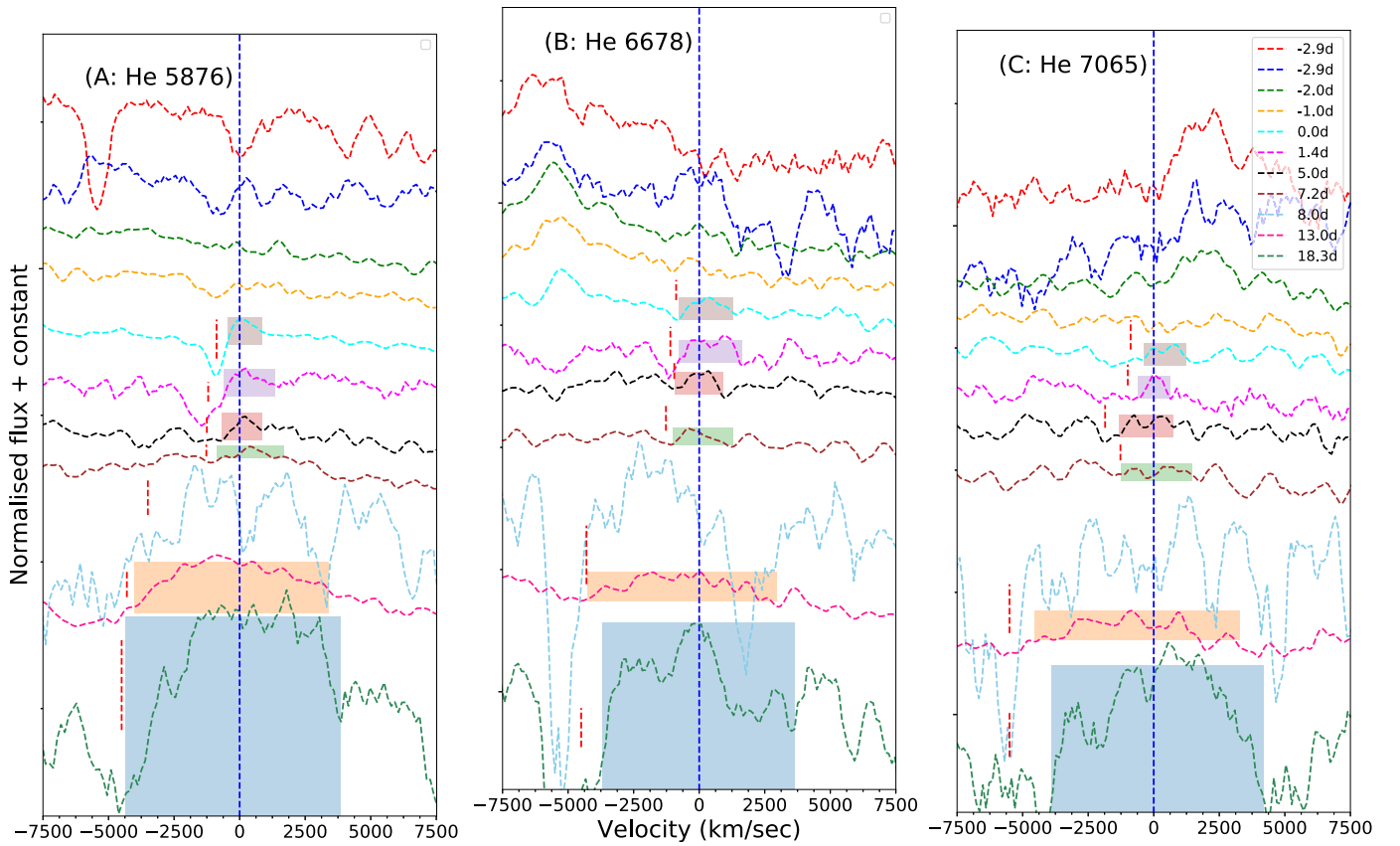


Figure 10. Line evolution of He I 5876, 6678, and 7065 Å. These lines broaden with time showing prominent evolution. The blue dotted line corresponds to the central velocity of 0 km s⁻¹. The red dotted line represents the absorption minima corresponding to the velocity estimations. The shaded regions in the plot describes the area used for the estimation of the EWs.

continuously photoionized by early ejecta-CSM interaction in the inner CSM regions and/or by the initial shock breakout. Once recombination occurs, the shell becomes transparent and we see the signatures of underlying SN ejecta and the spectrum is dominated by broad P cygni lines.

Figure 10 shows the evolution of the He I 5876, 6678, 7065 Å feature in the velocity space. We see a narrow P cygni profile which gradually evolves with time and shows a broad emission on top. The physical explanation behind the origin of the P cygni subclass could be a shell of He around the progenitor star surrounded by a dense CSM. As the optically thick shell is lit by the explosion, the narrow P cygni features transition to broader emission as the shell is swept up by the SN ejecta. The viewing angle dependence could also affect this scenario; if the CSM is asymmetric and, we have a He-rich torus, then P cygni features would only be visible if the system is viewed edge-on, while emission features can be seen only if it is viewed face-on. On the contrary, Karamehmetoglu et al. (2021) suggest that dominance of emission at late phases is not because of being optically thin, but because they lack other lines to branch into it. UV and X-ray emission arising at the shock boundary are the source of He ionization and recombination. The ionized region outside the shock leads to electron scattering and emission, P cygni features usually originate from optical depths ≤ 1 . X-rays penetrating further into the P cygni producing regions will fill in the absorption and lead to emission features. Thus, this provides an alternative scenario to the transitioning of P cygni to emission features of He I lines for SNe Ibn. Asymmetric CSM, thus, plays an

important role in the origin of these unusual features. Much of the ejecta usually moves undisturbed by the prevalent CSM configuration. Luminosity generation as a consequence of the interaction of the equatorial CSM beneath the photosphere continues, but, spectral signatures remain hidden until the photosphere recedes. This is the primary cause driving the blue continuum at early stages followed by the appearance of broadened redshifted He features (Andrews & Smith 2018).

We measure the expansion velocities and EWs of three neutral He lines (5876, 6678, and 7065 Å), wherever visible. The emission lines of He I were fit using a Gaussian on a linear continuum. The estimation of EW involves calculation of the integral of the flux normalized to the local continuum. We do not measure the EW of the P cygni lines. The velocities reported are estimated from the absorption minima of P cygni profiles. Figure 11 shows the evolution of velocity and EW for a sample of SNe Ibn taken from Hosseinzadeh et al. (2017). We see an increasing trend in both the line velocities and EW of the He lines. The velocity estimates of SN 2019wep lie at the upper range of SNe Ibn and show a faster evolution. In SN 2019wep, the broad features seen are more prominent than typical emission velocity of SNe Ibn around maxima varying between 6000 and 8000 km s⁻¹ (Hosseinzadeh et al. 2017). SN 2019wep has a good resemblance to ASASSN-15ed reaching broader emission profiles as seen in the P cygni subclass (Hosseinzadeh et al. 2017) while the emission subclass shows less evolution in line velocities. The EWs of the absorption component of He I lines for SN 2019wep are at an extreme high end than the normal SNe Ibn. This is also an

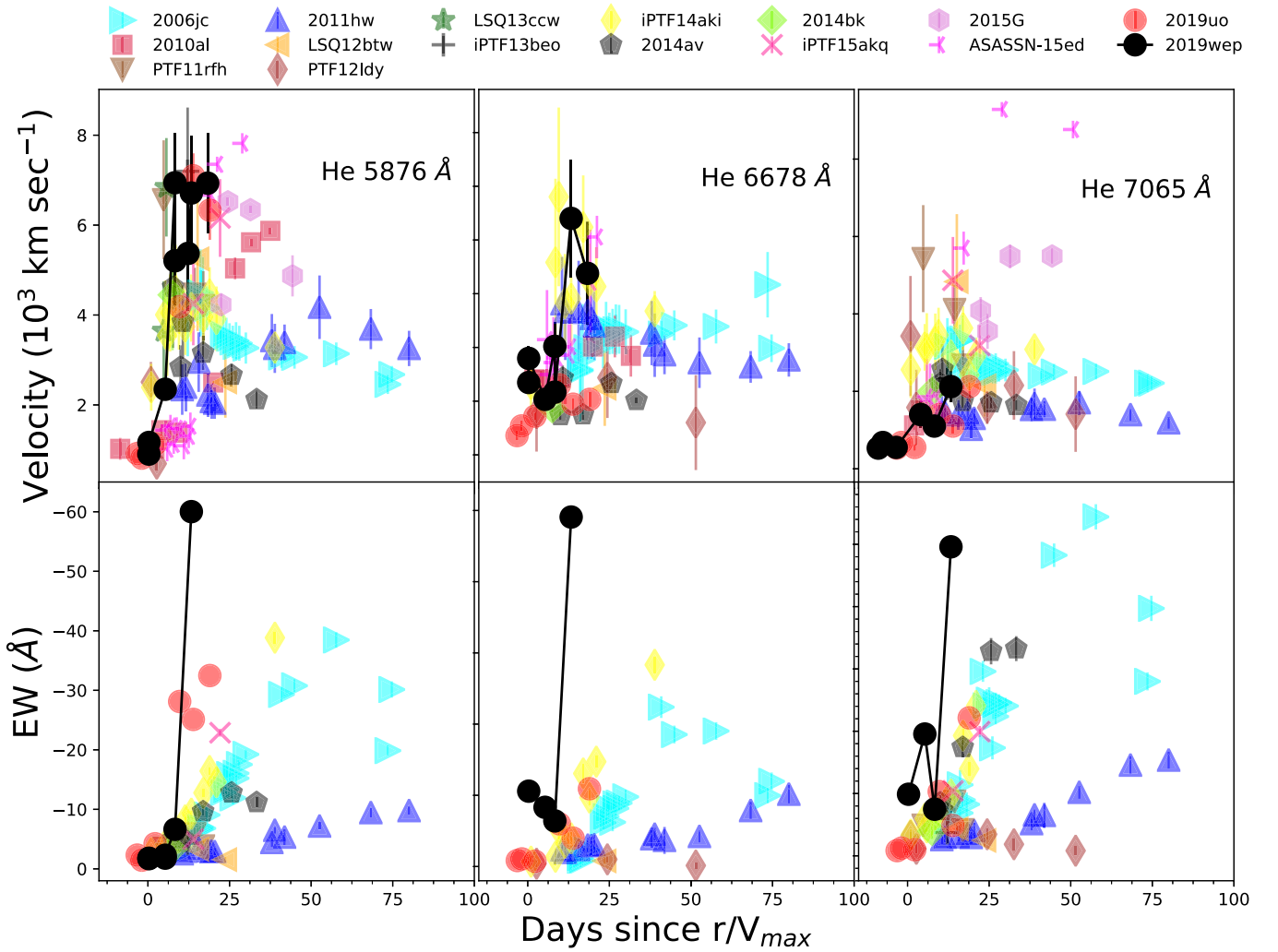


Figure 11. Evolution of line velocities and EWs of He I emission lines is shown in top and bottom panels, respectively. The data for this are taken from SNe 2006jc (Foley et al. 2007; Pastorello et al. 2008a), 2010al (Pastorello et al. 2015a), 2011hw (Pastorello et al. 2015a), PTF11rfh (Hosseinzadeh et al. 2017), LSQ12btw (Pastorello et al. 2015b), OGLE12-006 (Pastorello et al. 2015e), PTF12ldy (Hosseinzadeh et al. 2017), iPTF13beo (Gorbikov et al. 2014), LSQ13ccw (Pastorello et al. 2015b), iPTF14aki (Hosseinzadeh et al. 2017), 2014av (Pastorello et al. 2016), 2014bk (Pastorello et al. 2016), iPTF15akq (Hosseinzadeh et al. 2017), ASASSN-15ed (Pastorello et al. 2015c), 2015G (Hosseinzadeh et al. 2017), and 2019uo (Gangopadhyay et al. 2020a).

indication that perhaps SN 2019wep lies somewhere between SN Ib and SNe Ibn.

4.1. He I Line Velocity Evolution

A wide diversity and heterogeneity is observed in the spectral evolution of SNe Ibn in accordance with SNe IIn. The physical parameters of SNe Ibn strongly depend on the composition, geometry, mass, and density profile of CSM along with the residual stellar envelope at the time of explosion.

The properties of stellar wind and CSM can be inferred probing the line emitting regions. Spectra of interacting SNe IIn and SNe Ibn are typically produced in different gas regions (Chevalier & Fransson 1985; Chugai 1997). The emitting material moving at different velocities are indicated by different components of SNe with varying widths. The slow expanding, photoionized CSM is usually indicated by narrow emission lines (with velocities from a few hundreds to 6500 km s^{-1}). This gas is unshocked CSM produced by the progenitor star before exploding as an SN. This gives information on the mass-loss history of the SN progenitors.

When a clear P cygni profile is identified, the position of the core of the blueshifted absorption gives an idea of the expanding material. When this component is not detected, the velocity is estimated through the FWHM of the strongest He I emission lines, obtained after deblending the full line profile with Gaussian fits. Figure 12 shows the He I velocity of SN 2019wep, estimated from the weighted average of first two days to be $510 \pm 20 \text{ km s}^{-1}$. The expected range of W-R wind speeds ($500\text{--}3200 \text{ km s}^{-1}$) (Crowther & Smartt 2007) is shown as the purple shaded region, the expected wind speeds of LBV stars ($50\text{--}600 \text{ km s}^{-1}$) (Smith 2017) is shown in red and the expected wind speed range of RSG stars ($10\text{--}50 \text{ km s}^{-1}$) (van Loon et al. 2005) shown in black. Objects like SN 2019wep that show low CSM velocity are well matched with other low-velocity SNe 2011hw ($200\text{--}250 \text{ km s}^{-1}$) and 2005la (about 500 km s^{-1}). For such SNe, an H α line of moderate strength is also found to be associated with the SNe. Scenarios of H lines along with modest stellar wind velocities (a few hundreds kilometers per second) are compatible with stellar progenitors that are transitioning between the LBV and the W-R (WNE-type) stages (Pastorello et al. 2008b, 2015d, 2016). PS1-12sk is one such event that showed narrow He I lines and

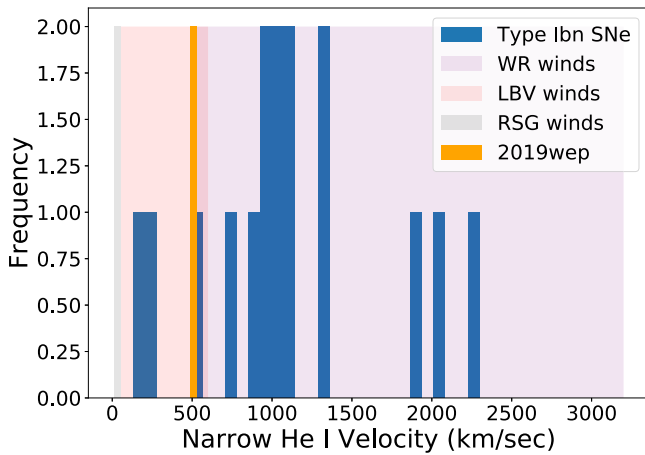


Figure 12. Histogram representing the sample of SNe Ibn taken from Pastorello et al. (2016) with blue bars. The orange shaded bar is the velocity with errors of SN 2019wep averaged over the first 2 days. The black, red, and purple shaded regions represent the wind speeds of RSG, LBV, and W-R stars respectively.

relatively weak intermediate-width $H\alpha$ lines and is uniquely associated with an elliptical galaxy. The plot also shows that the velocity of He I, represented by horizontal bars, lies at the lower end of the velocity distribution of SNe Ibn.

The traditional description by Humphreys & Davidson (1994) defines LBVs as single stars between 60 and 100 M_{\odot} at a transitional phase in the evolution of the most massive stars, between the main-sequence O-type stars and the H-deficient W-R stars. However, Smith & Tombleson (2015) found that the LBVs are surprisingly isolated from O-type stars. Smith & Tombleson (2015) further claimed that many LBVs are likely to be the product of binary evolution and cannot drive the mass-loss mechanism leading to a W-R phase. Humphreys et al. (2016) again reverted the scenario proposed by Smith & Tombleson (2015) highlighting their uneven sample and reconfirm that LBVs are evolved massive stars that have shed a lot of mass and are moving toward a W-R phase.

Following the above description both single and binary progenitor scenarios are equally likely in case of SN 2019wep with the progenitor having a reminiscent $H\alpha$ feature typical of LBV stars and gradually transitioning to a W-R phase having a dense CSM owing to the mass-loss rates of the LBV. It has been established that the sites of SNe Ibn are generally associated with star-forming environments (Pastorello et al. 2015a), with one exceptional case where no/little association of star formation activity was found (PS1-12sk; Sanders et al. 2013; Hosseinzadeh et al. 2019). Thus, the popular and speculative progenitors are typically single massive W-R stars with mass $\geq 18 M_{\odot}$ (Tominaga et al. 2008; Maeda & Moriya 2022) or a binary progenitor scenario, which may be equally likely (Foley et al. 2007).

4.2. Origin of the $H\alpha$ Feature

The $H\alpha$ feature originating in SNe serve as an important classifier among the interacting SNe group. Although narrow He I emission lines are frequently detected in the spectra of SNe IIn, the relative strengths between $H\alpha$ and the most prominent optical lines He I (5876 and 7065 Å) determines the classification of the transient as an SN IIn, SN Ibn, or even a transitional object between these two SN types.

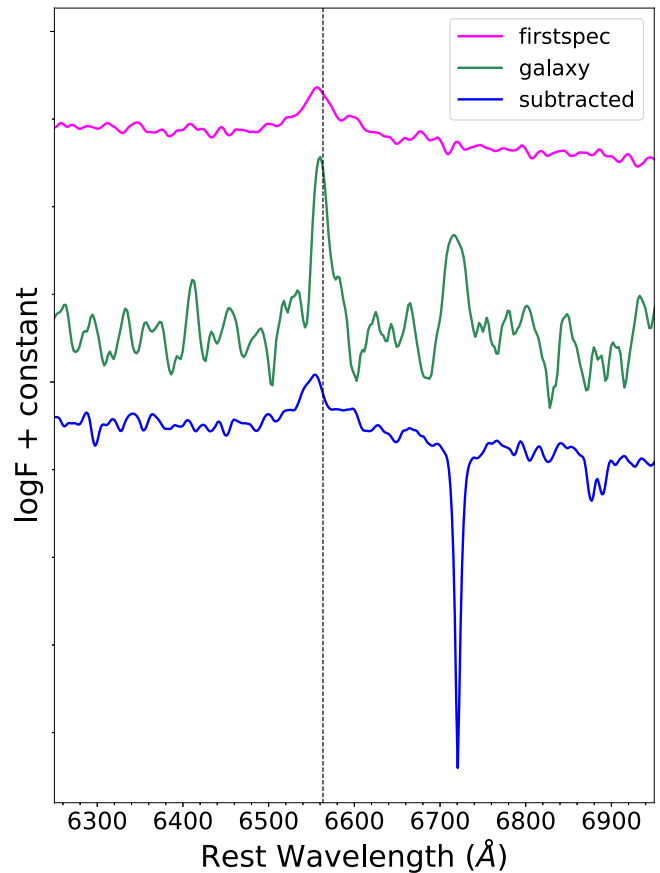


Figure 13. The first day, galaxy and subtracted spectra of SN 2019wep taken with the LCO networks. A reminiscent $H\alpha$ is seen in the subtracted profile.

In the two transitional SNe IIn/Ibn 2005la and 2011hw, Balmer lines were prominently detected (Pastorello et al. 2008b, 2015d, 2016). The strength of $H\alpha$ feature in both these SNe are comparable with He I lines. In the early spectrum of SN 2005la (Modjaz et al. 2014), $H\alpha$ showed a narrow, marginally resolved (FWHM $\sim 400 \text{ km s}^{-1}$) component, superposed on a broader base with a P cygni profile while the highest resolution spectrum of SN 2011hw (Pastorello et al. 2015d) showed an unresolved $H\alpha$ (FWHM $\leq 250 \text{ km s}^{-1}$) observed over a much broader wing and the intermediate $H\alpha$ component with FWHM monotonically increasing between 1350 and 2350 km s^{-1} . However, most of the SNe Ibn show no prominent $H\alpha$ lines or, in some cases, the identification of $H\alpha$ is controversial. For example, the detection of multiple lines of C II in the spectra of PS1-12sk, Sanders et al. (2013) argued—at least in the case of that object—against the identification of H lines.

We also see little $H\alpha$ at early time in SN 2019wep. To check whether the $H\alpha$ is from the host galaxy or is a reminiscent contribution from the SN, we obtained a spectrum in 2021 June the 2.0 m FTN. This was used as a host galaxy template for subtraction on the first spectrum of the SN obtained with the same instrumental setup. The flux of the $H\alpha$ feature was matched. The subtracted spectrum is shown in Figure 13. Even after spectral subtraction, we see a residual $H\alpha$ component with FWHM $\sim 1050 \text{ km s}^{-1}$. When comparing with the first LCO spectrum, it looks like that one also had a broad $H\alpha$ base, not present in the host spectrum. So, we propose that at least some (and perhaps all) of the narrow $H\alpha$ seen is from the host, but

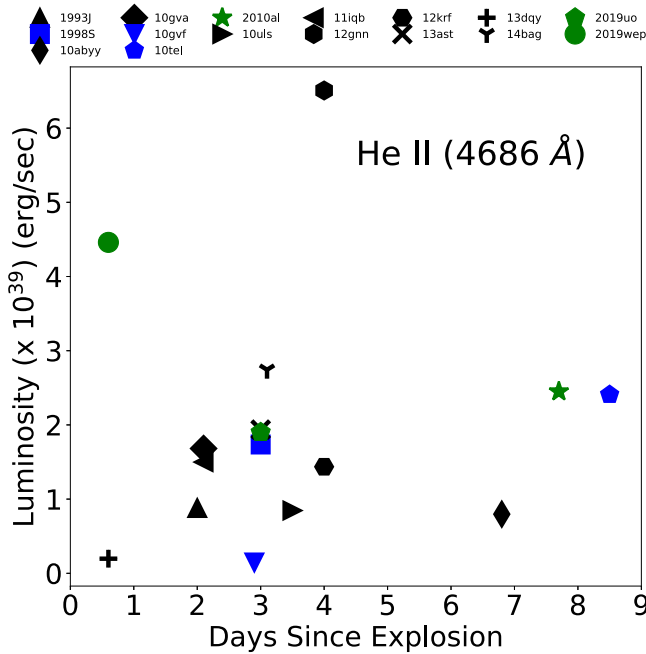


Figure 14. He II 4686 Å luminosity and EW of a sample of SNe showing flash ionization features in their early spectra with SNe II in black, IIn in blue, and Ibn in green (Khazov et al. 2016; Gangopadhyay et al. 2020a). SN 2019wep is shown as a green circle.

we cannot rule out that some of it (especially because there is a broad base) is from the SN. We, however, concur that there may be a contamination due to C II. In terms of spectroscopic properties, a transitioning behavior like SN 2011hw is noticed for SN 2019wep.

To ascertain the origin of SNe Ibn, a sample of 13 SNe II from literature (including SNe IIf, IIP, and IIn; Khazov et al. 2016) and Ibn (Hosseinzadeh et al. 2017; Gangopadhyay et al. 2020a), with flash ionization signatures within 10 days of explosion, are collected. The H lines are usually contaminated by host galaxy lines, so we therefore select the relatively isolated and unblended He II 4686 Å line. Since the He II lines are much narrower than the lines from the SN ejecta, they can serve as a good tool to probe the flash-ionized CSM. While measuring the luminosities, we remove the continuum by fitting a linear function. Figure 14 shows the typical luminosity of the He II line in SN 2019wep and other SNe II/IIn/Ibn. From the figure we see that only one SN along with SN 2019wep has been detected very early post explosion for which flash ionization signatures are detected owing to the recombination of CSM. The average luminosity of He II for SN 2019wep is higher than almost all other SNe II, IIn, and Ibn, which is indicative of the fact that the amount of CSM in SN 2019wep is larger than average SNe II, IIn, and Ibn samples at early time. This highlights the need for high-cadence SN spectroscopy at very early phase to detect signatures of flash ionization, which are also indicative of presence of CSM and will in turn be useful to infer the possible progenitors.

5. Summary

The paper summarizes the photometric and spectroscopic evolution of the SN Ibn 2019wep from -0.4 to 95 days post maximum. The availability of early data points in TNS were useful to constrain the V -band maxima. The light-curve decline is slower than the fast transients but is consistent with the



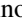




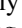

SNe Ibn group with a typical decay rate of $\sim 0.1 \text{ mag day}^{-1}$ (Hosseinzadeh et al. 2017). Fast transients are one of the exciting findings with characteristic timescales of ≤ 10 days, missed in most of the traditional surveys either due to poor resolution of the spectrum or unavailability of follow-up spectroscopic observations. A recent study by Ho et al. (2021) classified SNe Ibn as a subclass of fast transients due to their very similar rise times and blue continuum. This study motivated us to compare the properties of SN 2019wep with samples of SNe Ibn and fast transients. The limits on the absolute magnitude ($M_V = -18.26 \pm 0.20 \text{ mag}$ and $M_r = -18.18 \pm 0.95$) shows that the SN lies at the fainter end of SN Ibn subclass but is closer to the average absolute magnitude of the fast transients.

The correlation plots also suggest that the rise time of SN 2019wep is higher than that of the fast transients but is shorter than the average SNe Ibn value. Our analysis suggests that SN 2019wep decays fast and has low luminosity in comparison to other SNe Ibn. We quote the results of the bolometric light-curve modeling of SN 2019wep from Pellegrino et al. (2022). The bolometric light curve of SN 2019wep has striking resemblance with SN 2019uo suggesting a comparable ^{56}Ni mass in both SNe. The ejecta mass of SN 2019wep is consistent with SNe Ib samples, even though the models cannot be directly comparable because of different physical mechanisms involved. The low ^{56}Ni mass of SN 2019wep may suggest a significant fallback in the center, which can also possibly explain the consistency of the ejecta mass of SN 2019wep with the SNe Ib sample. The color evolution of SN 2019wep is unique, placing it between SNe Ib and SNe Ibn. The spectroscopic features of SN 2019wep indicate that it is one of the rare SNe Ibn with signatures of flash ionization. The early, prominent flash ionization lines of He II, C III, and N III are detected in the spectra, similar to SN 2019uo and SN 2010al. The disappearance of narrow He I features immediately after maximum and the transitioning to broad P cygni He I features hints toward a lateral shift from the SN Ibn to the SN Ib group. We interpret that the resemblance to SN Ib is due to the fact that the SN ejecta that is likely hidden by the CSM interaction becomes evident when the recombination comes into play at late phases. The P cygni subclass most likely originates from a He-rich shell around the progenitor surrounded by a dense CSM, or it may be due to viewing angle dependency. Asymmetry of the CSM configuration also plays a major role in this aspect. This is also validated by the EWs of He I features. The estimated line velocities are lower than the average values of SNe Ibn, but they show a faster evolution as compared to the emission subclass. The low He I velocity of CSM and the presence of residual $H\alpha$ in the spectroscopic features indicate that SN 2019wep is a transitional SN Ibn with progenitor scenario lying between an LBV and an W-R star. Maeda & Moriya (2022) essentially found that the progenitor of SNe Ibn are W-R stars with mass $\geq 18 M_\odot$. While Ho et al. (2021) estimate that the volumetric rate of SNe Ibn population is 0.5% of CCSNe, Maeda & Moriya (2022) with their updated estimations found that the volumetric rates is 1% of CCSNe population. This is of course below the fraction of SNe Ibn with masses $\geq 18 M_\odot$ but many of them are undetected in optical because of emission of large fraction of UV radiation for these candidate SNe (Maeda & Moriya 2022). High-cadence UV surveys are thus, quintessential to detect UV Ibn SNe population.

We thank the referee for several critical comments and useful suggestions that improved the presentation of the paper. We thank the support of the staff of the Xinglong 2.16 m and Lijiang 2.4 m telescopes for their support during observations. This work was partially supported by the Open Project Program of the Key Laboratory of Optical Astronomy, National Astronomical Observatories, Chinese Academy of Sciences. Funding for the Lijiang 2.4 m telescope has been provided by Chinese Academy of Sciences and the People's Government of Yunnan Province. We acknowledge Weizmann Interactive Supernova data REpository (WISEREP;<http://wiserep.weizmann.ac.il>). D.A.H. acknowledges support from NSF grant AST-1313404. The work of X.W. is supported by the National Science Foundation of China (NSFC grants 12033003, 11633002, and 11761141001), the Major State Basic Research Development Program (grant 2016YFA0400803), and the Scholar Program of Beijing Academy of Science and Technology (DZ:BS202002). This work makes use of data obtained from the LCO Network. K.M. acknowledges the BRICS grant DST/IMRCD/BRICS/Pilot-call/ProFCheap/2017(G) and the DST/JSPS grant, DST/INT/JSPS/P/281/2018 for the present work. I.A. is a CIFAR Azrieli Global Scholar in the Gravity and the Extreme Universe Program and acknowledges support from that program, from the European Research Council (ERC) under the European Union's Horizon 2020 research and innovation program (grant agreement No. 852097), from the Israel Science Foundation (grant No. 2752/19), from the United States–Israel Binational Science Foundation (BSF), and from the Israeli Council for Higher Education Alon Fellowship. J.Z. is supported by the NSFC (grants 12173082, 11773067), by the Youth Innovation Promotion Association of the CAS (grant 2018081), and by the Ten Thousand Talents Program of Yunnan for Top-notch Young Talents. The LCO team is supported by NSF grants AST-1911151 and AST-1911225.

Software: *lcogtspipe* (Valenti et al. 2011, 2016), *IRAF* (Tody 1986, 1993), *DAOPHOT* (Stetson 1987), *HOTPANTS* (Becker 2015), *superbol* (Lusk 2016).

ORCID iDs

Anjasha Gangopadhyay  <https://orcid.org/0000-0002-3884-5637>
 Kuntal Misra  <https://orcid.org/0000-0003-1637-267X>
 Griffin Hosseinzadeh  <https://orcid.org/0000-0002-0832-2974>
 Iair Arcavi  <https://orcid.org/0000-0001-7090-4898>
 Craig Pellegrino  <https://orcid.org/0000-0002-7472-1279>
 Xiaofeng Wang  <https://orcid.org/0000-0002-7334-2357>
 D. Andrew Howell  <https://orcid.org/0000-0003-4253-656X>
 Jamison Burke  <https://orcid.org/0000-0003-0035-6659>
 Jujia Zhang  <https://orcid.org/0000-0002-8296-2590>
 Koji Kawabata  <https://orcid.org/0000-0001-6099-9539>
 Mridweeka Singh  <https://orcid.org/0000-0001-6706-2749>
 Raya Dastidar  <https://orcid.org/0000-0001-6191-7160>
 Daichi Hiramatsu  <https://orcid.org/0000-0002-1125-9187>
 Curtis McCully  <https://orcid.org/0000-0001-5807-7893>
 Danfeng Xiang  <https://orcid.org/0000-0002-1089-1519>

References

Andreoni, I., Coughlin, M. W., Kool, E. C., et al. 2021, *ApJ*, 918, 63
 Andrews, J. E., & Smith, N. 2018, *MNRAS*, 477, 74
 Arcavi, I., Wolf, W. M., Howell, D. A., et al. 2016, *ApJ*, 819, 35

Becker, A. 2015, *HOTPANTS: High Order Transform of PSF ANd Template Subtraction*, Astrophysics Source Code Library, ascl:1504.004
 Bellm, E. 2014, in Proc. Third Hot-wiring the Transient Universe Workshop, ed. P. R. Wozniak, J. Graham, A. Mahabal, & R. Seaman, 27
 Bellm, E. C., Kulkarni, S. R., Barlow, T., et al. 2019, *PASP*, 131, 068003
 Benetti, S., Turatto, M., Valenti, S., et al. 2011, *MNRAS*, 411, 2726
 Bose, S., Dong, S., Kochanek, C. S., et al. 2018, *ApJ*, 862, 107
 Chatzopoulos, E., Wheeler, J. C., & Couch, S. M. 2013, *ApJ*, 776, 129
 Chevalier, R. A. 1982, *ApJL*, 259, L85
 Chevalier, R. A., & Fransson, C. 1985, in *Supernova Interaction with a Circumstellar Wind and the Distance to SN 1979c*, ed. N. Bartel, Vol. 224 (Berlin: Springer), 123
 Chugai, N. N. 1997, *Ap&SS*, 252, 225
 Clark, P., Maguire, K., Innes, C., et al. 2020, *MNRAS*, 492, 2208
 Cooke, J., Ellis, R. S., Nugent, P. E., et al. 2010, *ATel*, 2491, 1
 Crowther, P., & Smartt, S. 2007, *A&G*, 48, 1.35
 Drout, M. R., Chornock, R., Soderberg, A. M., et al. 2014, *ApJ*, 794, 23
 Fassia, A., Meikle, W. P. S., Chugai, N., et al. 2001, *MNRAS*, 325, 907
 Foley, R. J., Smith, N., Ganeshalingam, M., et al. 2007, *ApJL*, 657, L105
 Gal-Yam, A. 2014, *AAS Meeting Abstracts*, 223, 235.02
 Gal-Yam, A. 2019, *ApJ*, 882, 102
 Gal-Yam, A., Arcavi, I., Ofek, E. O., et al. 2014, *Natur*, 509, 471
 Gal-Yam, A., Bruch, R., Schulze, S., et al. 2022, *Natur*, 601, 201
 Gal-Yam, A., & Leonard, D. C. 2009, *Natur*, 458, 865
 Gangopadhyay, A., Misra, K., Hiramatsu, D., et al. 2020a, *ApJ*, 889, 170
 Gangopadhyay, A., Misra, K., Sahu, D. K., et al. 2020b, *MNRAS*, 497, 3770
 Gorbikow, E., Gal-Yam, A., Ofek, E. O., et al. 2014, *MNRAS*, 443, 671
 Groh, J. H. 2014, *A&A*, 572, L11
 Ho, A. Y. Q., Perley, D. A., Gal-Yam, A., et al. 2021, arXiv:2105.08811
 Hosseinzadeh, G., Arcavi, I., Valenti, S., et al. 2017, *ApJ*, 836, 158
 Hosseinzadeh, G., McCully, C., Zabludoff, A. I., et al. 2019, *ApJL*, 871, L9
 Huang, F., Li, J.-Z., Wang, X.-F., et al. 2012, *RAA*, 12, 1585
 Humphreys, R. M., & Davidson, K. 1994, *PASP*, 106, 1025
 Humphreys, R. M., Weis, K., Davidson, K., & Gordon, M. S. 2016, *ApJ*, 825, 64
 Karamahmetoglu, E., Fransson, C., Sollerman, J., et al. 2021, *A&A*, 649, A163
 Kasliwal, M. M., Kulkarni, S. R., Gal-Yam, A., et al. 2010, *ApJL*, 723, L98
 Khazov, D., Yaron, O., Gal-Yam, A., et al. 2016, *ApJ*, 818, 3
 Lusk, J. A. 2016, *SuperBol: Module for calculating the bolometric luminosities of supernovae*, Astrophysics Source Code Library, ascl:1609.019
 Lusk, J. A., & Baron, E. 2017, *PASP*, 129, 044202
 Lyman, J. D., Bersier, D., James, P. A., et al. 2016, *MNRAS*, 457, 328
 Maeda, K., & Moriya, T. J. 2022, *ApJ*, 927, 25
 Mao, X., Gao, W., Ding, Y., Zhang, M., & Gao, X. 2019, *TNSTR*, 2019-2556, 1
 Matheson, T., Filippenko, A. V., Chornock, R., Leonard, D. C., & Li, W. 2000, *AJ*, 119, 2303
 Modjaz, M., Blondin, S., Kirshner, R. P., et al. 2014, *AJ*, 147, 99
 Moriya, T. J., & Maeda, K. 2016, *ApJ*, 824, 100
 Morozova, V., Piro, A. L., & Valenti, S. 2017, *ApJ*, 838, 28
 Munari, U., & Zwitter, T. 1997, *A&A*, 318, 269
 Nicholl, M. 2018, *RNAAS*, 2, 230
 Nyholm, A., Sollerman, J., Tartaglia, L., et al. 2020, *A&A*, 637, A73
 Ofek, E. O., Rabinak, I., Neill, J. D., et al. 2010, *ApJ*, 724, 1396
 Pastorello, A., Benetti, S., Brown, P. J., et al. 2015a, *MNRAS*, 449, 1921
 Pastorello, A., Hadjiyska, E., Rabinowitz, D., et al. 2015b, *MNRAS*, 449, 1954
 Pastorello, A., Mattila, S., Zampieri, L., et al. 2008a, *MNRAS*, 389, 113
 Pastorello, A., Prieto, J. L., Elias-Rosa, N., et al. 2015c, *MNRAS*, 453, 3649
 Pastorello, A., Quimby, R. M., Smartt, S. J., et al. 2008b, *MNRAS*, 389, 131
 Pastorello, A., Smartt, S. J., Mattila, S., et al. 2007, *Natur*, 447, 829
 Pastorello, A., Tartaglia, L., Elias-Rosa, N., et al. 2015d, *MNRAS*, 454, 4293
 Pastorello, A., Vogl, C., Taubenberger, S., et al. 2021, *TNSAN*, 71, 1
 Pastorello, A., Wang, X. F., Ciabattari, F., et al. 2016, *MNRAS*, 456, 853
 Pastorello, A., Wyrzykowski, L., Valenti, S., et al. 2015e, *MNRAS*, 449, 1941
 Pellegrino, C., Howell, D. A., Vinkó, J., et al. 2022, *ApJ*, 926, 125
 Perley, D. A., Sollerman, J., Schulze, S., et al. 2022, *ApJ*, 927, 180
 Poznanski, D., Prochaska, J. X., & Bloom, J. S. 2012, *MNRAS*, 426, 1465
 Prentice, S. J., Ashall, C., James, P. A., et al. 2019, *MNRAS*, 485, 1559
 Prentice, S. J., Mazzali, P. A., Pian, E., et al. 2016, *MNRAS*, 458, 2973
 Pursiainen, M., Childress, M., Smith, M., et al. 2018, *MNRAS*, 481, 894
 Sanders, N. E., Soderberg, A. M., Foley, R. J., et al. 2013, *ApJ*, 769, 39
 Schlafly, E. F., & Finkbeiner, D. P. 2011, *ApJ*, 737, 103
 Schlegel, E. M. 1990, *MNRAS*, 244, 269
 Shivvers, I., Zheng, W. K., Mauerhan, J., et al. 2016, *MNRAS*, 461, 3057

- Silverman, J. M., Kleiser, I. K. W., Morton, A. J. L., & Filippenko, A. V. 2010, *CBET*, **2223**, 1
- Smith, N. 2017, in *Interacting Supernovae: Types IIn and Ibn*, ed. A. W. Alsabti & P. Murdin (Berlin: Springer), **403**
- Smith, N., Chornock, R., Silverman, J. M., Filippenko, A. V., & Foley, R. J. 2010, *ApJ*, **709**, **856**
- Smith, N., Foley, R. J., & Filippenko, A. V. 2008, *ApJ*, **680**, **568**
- Smith, N., & Tombleson, R. 2015, *MNRAS*, **447**, **598**
- Stetson, P. B. 1987, *PASP*, **99**, **191**
- Stritzinger, M., Mazzali, P., Phillips, M. M., et al. 2009, *ApJ*, **696**, **713**
- Strotjohann, N. L., Ofek, E. O., Gal-Yam, A., et al. 2021, *ApJ*, **907**, **99**
- Sun, N.-C., Maund, J. R., Hirai, R., Crowther, P. A., & Podsiadlowski, P. 2020, *MNRAS*, **491**, **6000**
- Taddia, F., Stritzinger, M. D., Bersten, M., et al. 2018, *A&A*, **609**, **A136**
- Taddia, F., Stritzinger, M. D., Sollerman, J., et al. 2013, *A&A*, **555**, **A10**
- Tampo, Y., Tanaka, M., Maeda, K., et al. 2020, *ApJ*, **894**, **27**
- Tody, D. 1986, *Proc. SPIE*, **627**, **733**
- Tody, D. 1993, in *ASP Conf. Ser. 52, Astronomical Data Analysis Software and Systems II*, ed. R. J. Hanisch, R. J. V. Brissenden, & J. Barnes (San Francisco, CA: ASP), **173**
- Tominaga, N., Limongi, M., Suzuki, T., et al. 2008, *ApJ*, **687**, **1208**
- Valenti, S., Fraser, M., Benetti, S., et al. 2011, *MNRAS*, **416**, **3138**
- Valenti, S., Howell, D. A., Stritzinger, M. D., et al. 2016, *MNRAS*, **459**, **3939**
- Valenti, S., Sand, D., Pastorello, A., et al. 2014, *MNRAS*, **438**, **L101**
- van Loon, J. T., Cioni, M. R. L., Zijlstra, A. A., & Loup, C. 2005, *A&A*, **438**, **273**
- Wang, S.-Q., & Li, L. 2020, *ApJ*, **900**, **83**
- Wang, X., Lin, W., Zhang, J., et al. 2021, *ApJ*, **917**, **97**
- Xiang, D., Wang, X., Lin, W., et al. 2021, *ApJ*, **910**, **42**
- Zhang, J., Ye, K., & Wang, X. 2019a, *TNSCR* **209-25651**, **1**
- Zhang, J., Ye, K., & Wang, X. 2019b, *ATel*, **13337**, **1**